Grid box-level evaluation of IMERG over Brazil at various space and time scales

André N. Gadelha[a,*], Victor Hugo R. Coelho[a,*], Alexandre C. Xavier[b], Luís Romero Barbosa[a,c], Davi C. D. Melo[d,e], Yunqing Xuan[f], George J. Huffman[g], Walt A. Petersen[h], Cristiano N. Almeida[a]

[a] Department of Civil and Environmental Engineering, Federal University of Paraíba, João Pessoa, PB 58051-900, Brazil

[b] Department of Rural Engineering, Federal University of Espírito Santo, Alegre, ES 29500-000, Brazil

[c] Institute of Earth and Environmental Science, University of Potsdam, Potsdam, BB 14476, Germany

[d] Department of Soils and Rural Engineering, Federal University of Paraíba, Areia, PB 58397-000, Brazil

[e] Department Hydraulics and Sanitary Engineering, University of São Paulo, São Carlos, SP 13566-590, Brazil

[f] College of Engineering, Swansea University, Swansea, SA1 8EN, UK

[g] NASA Goddard Space Flight Center, Greenbelt, MD 20771, USA

[h] NASA Marshall Space Flight Center, Huntsville, AL 35805, USA

* Corresponding authors. Tel.: +55-83-3216-7684.

E-mail addresses: andregadelha5@hotmail.com (A.N. Gadelha), victor-coelho@hotmail.com (V.H.R. Coelho), alexandre.xavier@ufes.br (A.C. Xavier), luisromero.eng@gmail.com (L.R. Barbosa), melo.dcd@gmail.com (D.C.D. Melo), y.xuan@swansea.ac.uk (Y. Xuan), george.j.huffman@nasa.gov (G.J. Huffman), walt.petersen@nasa.gov (W.A. Peterson), almeida74br@yahoo.com.br (C.N. Almeida).

ABSTRACT: Rainfall data from the Global Precipitation Measurement (GPM) mission provide a new source of information with high spatiotemporal resolution that overcomes the limitations of ground-based rainfall information worldwide. This study evaluates the performance of the Integrated Multi-satellitE Retrievals for GPM (IMERG) Final Run product over Brazil by means of multi-temporal and -spatial analyses. The assessment of the IMERG Final Run product is based on six statistics obtained for the period between January-December 2016 (daily, monthly, and annual basis). The analysis consisted of comparing the satellite-based

estimates against a ground-based gridded rainfall product created using daily records from 4,911 rain gauges distributed throughout Brazil. Overall, the results show that the IMERG product can effectively capture the spatial patterns of rainfall across Brazil. However, the IMERG product presents a slight tendency in overestimating the ground-based rainfall at all timescales. Furthermore, the performance of the satellite varies throughout the regions. The higher errors and biases are found in the North and Central-West regions, but the low density of rain gauges in those regions can be a source of large deviations between IMERG estimates and observed data. As well, a large underestimation of the IMERG data is evidenced along the coastal zone of the Northeast region, probably due to the inability of the passive microwave and infrared sensors to detect warm-rain processes over land. This study shows that the IMERG product can be a good source of rainfall data to complement the ground precipitation measurements in most of Brazil, although some uncertainties are found and need to be further studied.

Keywords: Gridded rainfall, Global Precipitation Measurement, Final Run, Performance

1. Introduction

Rainfall plays an important role in the water balance, as it is the main input into the hydrological system (Kidd and Huffman, 2011; Mahmoud et al., 2018; Schneider et al., 2016). Given its spatial and temporal variability, dense daily or sub-daily observations are required to understand specific hydrological processes (Kann et al., 2015; Kidd et al., 2017; McMillan et al., 2011; Meng et al., 2014). However, obtaining a consistent and continuous ground-based rainfall dataset with an adequate spatiotemporal resolution for such purposes remains a challenge worldwide, mainly because of the costs of operation and maintenance of the rain gauge monitoring network (Terink et al., 2018). Currently, the ground-based rainfall monitoring network in Brazil has approximately 11,820 rain gauges, resulting in an average density of one gauge per 720 km^2, which is below the threshold of one gauge per 575 km^2 recommended by the World Meteorological Organization (WMO) for the interior plane and undulating areas (WMO, 1994). However, the gauges are non-uniformly distributed with some regions in Brazil, such as the Southeast, having densities much higher than the threshold, reaching one gauge per 115 km^2. Moreover, rain gauges with uninterrupted data in Brazil are few and the rainfall time series often contain temporal gaps. The lack of in-situ rainfall data is more acute in the Northern (which includes the

Amazon rainforest) and Central regions of the country, leading to an insufficient characterisation of these regions (Buarque et al., 2011; Collischonn et al., 2008; Curtarelli et al., 2014; Delahaye et al., 2015).

Precipitation observations by alternative methods such as multiple satellite sensors have become a viable solution in the past few decades to overcome the limitations of ground-based data (Hobouchian et al., 2017; Levizzani et al., 2018; O and Kirstetter, 2018). Remotely sensed data can offer global information about precipitation with a range of required spatial and temporal resolutions. Furthermore, many remote sensing products related to rainfall are freely available for the end users (Mahmoud et al., 2018; Skofronick-Jackson et al., 2018; Tang et al., 2016a). One of the first dedicated and most important satellites for this purposes was the Tropical Rainfall Measuring Mission (TRMM), launched in 1997. It was a joint project between NASA (National Aeronautics and Space Administration) and JAXA (Japanese Aerospace Agency) to observe rainfall in the latitude band 50º North to 50° South (Huffman et al., 2007). TRMM provided products with a variety of spatial (0.25º to 5º) and temporal (3-hour to 1-month) resolutions. In the past few years, many studies used the TRMM Multi-satellite Precipitation Analysis (TMPA) for various purposes in Brazil such as hydrological modelling due to the low density and intermittency of rain gauges in some river basins (e.g. Coelho et al., 2017; Collischonn et al., 2008; De Paiva et al., 2013; Falck et al., 2015; Melo et al., 2016). Many other studies worldwide were also carried out using the TMPA (including Baik and Choi, 2015; Fang et al., 2013; Naumann et al., 2012; Pombo and de Oliveira, 2015; Yang and Nesbitt, 2014). However, some studies highlighted the need to assess the accuracy of the TMPA by comparison with ground-based data on a regional basis. For example, Melo et al. (2015) evaluated the TMPA over Brazil using a 14-year time series for uncertainties in daily and monthly estimates.

Like TRMM, the Global Precipitation Measurement (GPM) mission is also a joint project led by NASA and JAXA; the GPM Core Observatory launched in February 2014. GPM is the successor to TRMM, providing rainfall and snow information globally as contained in the Integrated Multi-satellitE Retrievals for GPM (IMERG) products at 0.1º x 0.1º (spatial) and half-hour (temporal) resolutions (Hou et al., 2014; Liu et al., 2017; Skofronick-Jackson et al., 2017). The IMERG algorithm incorporates microwave and infrared estimates from the GPM constellation, gauge observations, and other ancillary (Huffman et al., 2017a). Currently, there are three IMERG products available, namely: Early Run, Late Run, and Final Run. The Early and Late Run are near-real-time products available from 4 to 12 h after the observation, both being more suitable

for time-sensitive applications. On the other hand, the Final Run product is available 3.5 months after the observation, which allows it to incorporate a surface gauge analysis from the Global Precipitation Climatology Centre (GPCC) to improve the satellite estimations. As such, the Final Run is the most suitable product for hydrological modelling purposes (Tang et al., 2016b).

The GPM opens up new opportunities for hydrological investigations, particularly in ungauged areas (Asong et al., 2017). However, the performance of the GPM products needs to be critically evaluated in different regions of the world as sources of information for both end users and data producers (Prakash et al., 2018). Several recent studies evaluated different IMERG products in complex areas under distinct climatic and geographic aspects worldwide by using ground-based data and/or comparisons with other satellite products such as TMPA (Anjum et al., 2018; Asong et al., 2017; Beria et al., 2017; Dezfuli et al., 2017; Gebregiorgis et al., 2018; Lelis et al., 2018; Mahmoud et al., 2018; Mayor et al., 2017; Mitra et al., 2018; Muhammad et al., 2018; O and Kirstetter, 2018; Oliveira et al., 2018; Prakash et al., 2018, 2016; Satgé et al., 2017; Sungmin et al., 2017; Tan et al., 2017; Tan and Duan, 2017; Tan and Santo, 2018; Tang et al., 2016a, 2016b; Wang et al., 2017; Zhang et al., 2018). Most of the aforementioned studies showed good agreement of the IMERG products with the gauge, radar, and TMPA data. However, other studies found the same or less accuracy for the IMERG products compared to those from TMPA (Satgé et al., 2017). Some studies mentioned above were carried out at country-wide scale. Table 1 provides a tabular literature review which shows these relevant country-scale studies evaluating the performance of IMERG products, including those done in Brazil. It is the case that countries such as Brazil and China encompass different climate zones and rainfall patterns due to their vast territories. Consequently, studies carried out in these countries may be able to provide more detailed and critical analyses of the IMERG products.

INSERT TABLE 1

Table 1 Summary of relevant studies that evaluated the IMERG products at country-wide scale in relation to the proposed study.

As IMERG products have only become available recently, the number of studies carried out in Brazil from local-to national-scales is still very small. To our knowledge, only four studies checked the quality of the IMERG products (e.g. Lelis et al., 2018; Oliveira et al., 2018, 2016; Rozante et al., 2018), which are

111 significantly fewer than those that evaluated the TRMM products. For instance, Oliveira et al. (2016) used
112 ground-based radar observations to evaluate the rainfall variations of the IMERG Final Run Version 04 product
113 over an area of the Brazilian Amazon rainforest. They observed a satisfactory agreement between the ground-
114 based and the satellite data during the period analysed (from March to September 2014), but IMERG Final
115 overestimated the heavier rainfall rates during the wet season. Lelis et al. (2018) analysed the one-year
116 performance of the IMERG product by using rain gauges data for the eastern region of São Paulo State, Brazil.
117 They concluded that the IMERG product generally overestimated over this region. The only national-scale
118 assessment was carried out by Rozante et al. (2018), using around 3,400 rain gauges distributed over Brazil.
119 They analysed whether the daily IMERG data can properly replace the daily TMPA data. However, they
120 considered as a reference for the analyses of both products the coarse spatial resolution (0.25º) of the TMPA.
121 Moreover, they based their studies in a point-to-cell perspective, i.e. without a spatial analysis and considering
122 only 1,779 cells of the IMERG product among the more than 70,000 available for the Brazilian territory.
123 Clearly, the validation of satellite rainfall data based on a point-to-cell analysis has some limitations, as the
124 gauge stations provide point measurements observed over a continuous period of time, whereas precipitation
125 from satellite observation is an average within the grid cells (Cohen Liechti et al., 2012; Jesus et al., 2015; Toté
126 et al., 2015; Zad et al., 2018). Consequently, the comparison suffers from scale mismatch issues and other
127 validation methods are needed to improve the analyses and overcome this problem (Guo and Liu, 2016).
128 Considering the limitations of the previous studies assessing the IMERG products in Brazil, our aim
129 is to expand the analyses of the IMERG Final Run product across the Brazilian territory, as follows: (1) using
130 a grid box approach based on a gridded observed rainfall product, (2) including spatially varying analyses, and
131 (3) encompassing other variables in the evaluation process such as climate, topography, and density of observed
132 data used in the analyses. The IMERG product was compared with a large amount of daily ground-based
133 measurements distributed over grids covering the country, with grid boxes matching the IMERG cells. We
134 addressed the following questions in this study: (a) Can the IMERG product be used as a source of rainfall data
135 over Brazil? (b) How does the quality of the IMERG product vary spatially? (c) Are the annual and monthly
136 IMERG rainfall estimates more accurate than daily estimates? (d) What analysed variables have more influence
137 on the performance of the IMERG product? In the end, this study intends to provide insights for further
138 applications of the IMERG Final Run product in Brazil at daily, monthly, and annual scales.

2. Material and methods

2.1 Study area

This study was carried out for the whole Brazil, which covers approximately 8.5 M km^2 between the coordinates 5º16´N-33º45´S and 34º47´W-73º59´W (Fig. 1). Brazil is the largest country in Latin America and the fifth-largest country in the world in area. The Brazilian territory has five official geographical regions, namely: North (N), Northeast (NE), Central-west (CW), Southeast (SE), and South (S). These regions generally correspond to the spatial variations in the long-term mean annual rainfall in Brazil. Region N, where the Amazon rainforest is located, is characterised by prevailing convective rainfall that can be higher than 2,000 mm year^{-1} and even reaches 4,000 mm year^{-1} in some places (Alvares et al., 2013; Espinoza Villar et al., 2009). In contrast, most of region NE is characterised by a semi-arid climate in the inland area, with rainfall ranging from 380 to 700 mm year^{-1} (Alvares et al., 2013). However, along the first 100 km of the Atlantic coastal zone of NE, the rainfall can be as high as 1,500 mm year^{-1} (Kousky, 1979). The annual rainfall variations are similar in both regions SE and CW, with values ranging from 1,000 to 2,000 mm and concentrated during the austral summer (Melo et al., 2015). On the other hand, the rainfall is more spatially uniform throughout the year in region S, ranging from 1,200 to 2,000 mm (Nery and Carfan, 2014). According to Alvares et al. (2013), Brazil has twelve different Koppen's climate types divided into three zones: Tropical (Zone A), Semiarid (Zone B), and Humid Subtropical (Zone C). The mean annual air temperature ranges from less than 10º C to greater than 26º C. Besides Brazil as a whole, five different subareas with the same size (1.9º x 1.2º) were also selected to be individually evaluated in this study to check the quality of the IMERG data in small areas with high density of rain gauges (Fig. 1b). Each subarea is located in one of the five official geographical regions and represents different climate zones and/or annual average rainfall depths. Only subarea 2 is meridionally oriented in order to be confined to the Dry Zone and to cover as many rain gauges as possible. Fig. S1 shows the long-term monthly average rainfall obtained from rain gauges within the five selected subareas.

INSERT FIG. 1

Fig. 1 (a) Number and density of rain gauges used as a reference in the study. (b) Köppen's climate classification map for Brazil according to Alvares et al. (2013) and selected subareas. Spatial distributions of the annual

rainfall (mm) for 2016 obtained from (c) rain gauges and (d) the IMERG-V05 Final product. The climatic symbols A, B, and C stand for Tropical, Dry, and Humid Subtropical, respectively.

2.2 Rain gauge data

This study used daily rainfall data from 4,911 rain gauges distributed over Brazil (Fig. 1). The ground-based data for 2016 were acquired from rain gauges that are operated by the Brazilian National Water Agency (ANA), Brazilian National Institute of Meteorology (INMET), and sixteen regional water agencies. The Angular Distance Weighting (ADW) interpolation method was used to produce a daily gridded observed rainfall data matching the 0.1º x 0.1º IMERG grid (Hofstra and New, 2009; New et al., 2000; Xavier et al., 2016). Following the recommendation by Xavier et al. (2016), the weighting means data from the five available surrounding stations were used when applying the ADW method to perform the point-to-grid conversion. The weights for each station were defined by two components: (1) the weight due to the distance from the grid point to the rain gauge, calculated by the correlation decay distance (CDD) and (2) the weight of each station due to its isolation. Detailed information of the interpolation method can be found in Xavier et al. (2016). The gauge data were quality checked for extreme daily values equal to or higher than 450 mm. The missing data throughout the year 2016 represents ~10% of the total dataset recorded in the rain gauges. Gauges with missing data for a specific day were excluded from the interpolation to generate the gridded rainfall product for that day. Hence, the number of rain gauges changed over the study period, ranging from 2,975 to 3,739 for each day. The daily data were then accumulated to produce the monthly and annual information.

2.3 IMERG data

The IMERG dataset evaluated in this study is the Final Run product at the native 0.1º x 0.1º (spatial) and half-hour (temporal) resolution; Version 05 (V05) of the Goddard Profiling Algorithm (GPROF V05) provides precipitation estimates from all microwave sensors onboard the GPM constellation. The main changes between the oldest and newest versions of the IMERG products are summarised by Huffman et al. (2017b). For instance, the IMERG-V05 improved the gauge error estimates to provide proper weighting of monthly gauge and satellite-only estimates. Also, the IMERG-V05 product added the Quality Index for all half-hour and monthly products. The IMERG-V05 Final Run product also uses the GPCC analysis of global ground-based

monthly data from the Global Telecommunication System (GTS) and other sources, which is composed of 7,000 stations distributed around the world. This study compared gauge and satellite-based data independently by choosing ground-based stations not used by GTS. The comparisons between the IMERG-V05 and rain gauge datasets were performed in this study at daily, monthly, and annual scales. Therefore, we aggregated the 30-minute IMERG-V05 data to match the daily information of the ground-based data, which is collected at 9:00 a.m. local time. The IMERG-V05 data were then accumulated between 9:00 a.m. (local time) and the subsequent 24 hours. Similar to the rain gauge data, the daily IMERG-V05 information was monthly and annually accumulated.

2.4 Evaluation procedures

Four evaluation procedures were performed to analyse the IMERG-V05 product over the Brazilian territory, so-called: (i) grid-scale, (ii) national-scale, (iii) subarea, and (iv) categorical analysis. The grid-scale comparison was carried out using the observed rainfall dataset and the IMERG-V05 product to evaluate the spatial behaviour of the satellite data. The national-scale analysis was performed to asses the satellite product over large areas comparing the national areal average of both ground-based and IMERG-V05 data. The subarea analysis consisted of computing the metrics of average values within each subarea defined in the study area section (see Fig. 1b). This analysis intends to assess how the IMERG-V05 performs in areas with a high density of gauges in each Brazilian region. The categorical analysis was carried out to better understand the spatial daily agreement between IMERG-V05 and observed rainfall data, based on the influence of climate, topography, and gauge density. The comparisons between the IMERG-V05 and rain gauge datasets were performed in this study at daily, monthly, and annual scales.

2.5 Metrics

Six statistical metrics divided into three main groups were used to assess the quality of the IMERG-V05 product. Considering the temporal resolution of the rain gauge network, the threshold for all daily metric analyses was set to 0.1 mm. Thus, all IMERG-V05 and/or rain gauge data with daily values below 0.1 mm were treated as zero. However, for the monthly and annual analyses, this threshold was not applied because it is of no physical sense. The first group of metrics is related to comparison of detecting the observed rainfall events,

including: (i) probability of detection (POD), which exhibits the fraction of rainfall events that the IMERG-V05 detects and there are ground-based rainfall events; (ii) false alarm ratio (FAR), which gives the fraction of events estimated by IMERG-V05 which are not detected in the surface data; and (iii) critical success index (CSI), which combines the characteristics of false alarms and missed events:

$$\mathrm{POD} = \frac{a}{a + c} \quad (1)$$

$$\mathrm{FAR} = \frac{b}{a + b} \quad (2)$$

$$\mathrm{CSI} = \frac{a}{a + b + c} \quad (3)$$

where a is the rainfall observed by the rain gauge and IMERG-V05 simultaneously, b is the rainfall observed by the IMERG-V05 but not observed by the rain gauge, and c is the rainfall observed by the rain gauges which was not observed by the satellite. Table 2 shows the definition of rainy and non-rainy days as well as each variable presented in Eqs. (1), (2), and (3). The desirable values of POD and CSI are close to one, while for FAR is near to zero.

INSERT TABLE 2

Table 2 Definition of rainy and non-rainy days for IMERG-V05 and observed data.

The second group of metrics corresponds to the errors of the IMERG-V05 estimation in comparison with the rain gauge data. It includes: (i) the mean error (ME), which represents the average magnitude of the satellite error, and (ii) the root mean square error (RMSE), which gives the sample standard deviation of the differences between the IMERG-V05 product and the observed rainfall:

$$\mathrm{ME} = \frac{1}{N}\sum_{n=1}^{1}(E_i - O_i) \quad (4)$$

$$\mathrm{RMSE} = \sqrt{\frac{1}{N}\sum_{i=1}^{n}(E_i - O_1)^2} \quad (5)$$

where O is the observed rainfall (mm), E is the IMERG-V05 estimated rainfall (mm), i is the index of the number of pairs, and n is the total number of compared pairs. Both ME and RMSE measure the accuracy of the IMERG-V05 product, so values close to zero indicate smaller errors. However, the ME gives an overall indicator of the bias (positive or negative), with the disadvantage that the positive and negative errors can cancel each other. Hence, sometimes a small ME does not means minor errors. The relative errors for both ME and

RMSE metrics were also computed to improve the interpretation of data (see the supplementary material for more details).

The third group describes the agreement between IMERG-V05 estimates and ground-based data, which only includes the correlation coefficient (CC):

$$CC = \frac{\frac{1}{n}\sum_{n+1}^{N}(O_i - \overline{O})(E_i - \overline{E})}{\sigma_O \sigma_E} \quad (6)$$

where $\bar{O}$ is the average observed rainfall values (mm), $\bar{E}$ is the average estimated rainfall values (mm), and σ is the standard deviation (mm). The CC ranges from +1 to -1, with the extremes representing total positive and total negative linear correlation, respectively.

3. Results and discussion

3.1 Grid-scale evaluation

In this analysis, the IMERG-V05 data was evaluated against the observed rainfall on the native 0.1° x 0.1° IMERG grid. The spatial distributions of POD and CSI suggest a good agreement of the IMERG-V05 in detecting daily rainfall events in most parts of Brazil, with values generally higher than 0.6 for both metrics (Fig. 2). The exception is along the eastern coast of the Brazilian NE, with many cells presenting values lower than 0.45 for both analysed metrics. The poor POD over coastal areas has also been observed in other studies of IMERG (e.g. Asong et al., 2017; Caracciolo et al., 2018). The FAR measures show that the IMERG-V05 product exhibited low false alarms at a daily scale, except for the central part of the NE along the Brazilian driest zone. This effect was probably caused by the low number of rainy days during the study period, as also noticed by Prakash et al. (2018) over southeast peninsular India due to the rain-shadow effects.

The spatial distribution of daily CC shows a good agreement of the IMERG-V05 product with the observed gridded data, wherein most cells presented values equal to or higher than 0.7 (Fig. 2d). The good agreement is more noticeable in the regions S, SE, and part of the NE. The exception in the region NE was observed along the Atlantic coastal zone, with CC ≤ 0.40 in some cells. This occurred because the IMERG-V05 failed to detect some rainfall events in the NE coast, as mentioned in the POD analysis. Melo et al. (2015) also observed poor agreement along the NE coastal region evaluating the daily rainfall data of TMPA products using

14-years time series. Similarly, Rozante et al. (2018) also detected large daily underestimation in most cells considered for the Brazilian coastal region by analysing IMERG and TMPA products. On the other hand, the worst agreement between the daily IMERG-V05 product and the gridded observed rainfall data was detected across the regions N and CW, with a large number of cells presenting CC values ranging from less than 0.1 to 0.6.

The spatial distribution of the IMERG-V05 product errors over Brazil shows that the ME values range between -5.5 (-75%) and 4.5 (110%) mm at daily temporal resolution analysis (Fig. 2e). The largest absolute underestimation and overestimation of the satellite data were observed in the region N for both ME and RMSE error metrics. This fact was expected because the North region, where the Amazon forest is located, is characterised by the largest amount of rainfall throughout the year. However, the range of relative ME and RMSE for region NE (from -75 to 110% and from 130 to 750%, respectively) is larger than the North region (from -60 to 90% and from 100 to 400%, respectively) (see Fig. S2). This effect can be observed along the coastal zone of the Brazilian NE, where considerable underestimation of the ME (higher than ~1 mm) was also detected, following the similar characteristics of the POD and CSI which presented low detection in the cells of the area.

INSERT FIG. 2

Fig. 2 Spatial distributions of daily (a) FAR, (b) POD, (c) CSI, (d) CC, (e) ME, and (f) RMSE.

Fig. 3 shows the box plots of metrics for the daily comparison for all of Brazil, where each point represents one analysed cell. The box delimits the first (25%) and third (75%) quantiles, while the strip and cross inside symbolise the median and mean, respectively. The whiskers indicate the 10 and 90% percentiles, with the circles after that representing the outliers. Overall, the three metrics related to detection of observed rainfall events show symmetric results close to each mean (Fig. 3a, b, and c). More than 90% of the cells presented values higher than 0.60 for POD and less than 0.22 for FAR, which indicates the good skill of the IMERG-V05 product in detecting daily rainfall over most of Brazil. The CC shows that most values are concentrated from 0.5 to 0.8, demonstrating a moderate agreement between observed and estimated rainfall grid values (Fig. 3d). Only 10% of the cells exhibited a CC lower than 0.4 for the daily analysis. The ME also showed strong symmetry at daily temporal resolution, with the mean close to 0 mm (Fig. 3e). This low ME

296 value may have been influenced by compensating positive and negative differences, as also observed by Tang
297 et al. (2016a) in China. The RMSE was relatively high when compared to ME because there is no plus/minus
298 compensation, with a mean value up to 7 mm for the evaluation of the IMERG-V05 product at grid scale. The
299 relative mean of the daily ME and RMSE represent 5 and 200%, respectively (see Fig. S2). This indicates a
300 small net bias, but potentially large uncertainty.

301 **INSERT FIG. 3**

302 **Fig. 3** Box plots of metrics over observed and estimated rainfall grids at daily temporal resolution: (a) FAR, (b)
303 POD, (c) CSI, (d) CC, (e) ME, and (f) RMSE. The histograms show the distribution of cells for each metric.
304

305 The monthly distribution of the metrics shows a noticeable improvement of the IMERG-V05 product
306 when compared with the daily analysis (Fig. 4). This behaviour confirms longer time averages are more
307 representative, as also seen by Caracciolo et al. (2018), Mayor et al. (2017), Tan et al. (2017), Tang et al.
308 (2016a), among others. Overall, the CC presented values higher than 0.80 for 90% of the cells available for the
309 Brazilian territory in the monthly analysis, most of them concentrated close to the mean (CC = 0.92) (Fig. 4a).
310 As at the daily scale, the monthly results indicate a poor agreement between rain gauges and satellite rainfall
311 grids observed over the N region and along the Atlantic coastal zone in NE, with CC reaching 0.3 in many cells.
312 For the NE coastal zone, an underestimation of the satellite data was observed. Such underestimation was most
313 likely caused by the prevalence of warm-rain process-dominated systems forced by the topography, which are
314 not well-detected by the passive microwave sensors over land, as noted by Rozante et al. (2018) and analysed
315 by Palharini and Vila (2017). Also, the calibration that works for infrared estimates in other places fails in NE
316 Brazil and is more prone to missing heavy events due to the weakness of cloud top-rain relationship, even if it
317 were calibrated correctly in an average sense. These factors presumably also drive the daily results reported
318 above.

319 As for the daily analysis, the monthly distribution of ME exhibited symmetric values concentrated
320 close to the mean (~2 mm), with 50% of the sample ranging from -8 to +16 mm (Fig. 4b). Once again, the low
321 average found for ME indicates cancellation between negative and positive values. The spatial distribution of
322 monthly ME shows that the extreme values larger than +60 mm and lower than -60 mm are more concentrated

in region N, which is echoed in the spatial distribution of RMSE. The mean relative ME and RMSE for monthly values are 5 and 36%, respectively (see Fig. S3).

INSERT FIG. 4

Fig. 4 Spatial distributions of monthly (a) CC, (c) ME, and (e) RMSE. Box plots and histograms of monthly (b) CC, (d) ME, and (e) RMSE.

Overall, the comparison between the annual rainfall grids shows that the IMERG-V05 product is fairly effective at representing the pattern of rainfall over Brazil (see Fig. 1c and d). However, some discrepancies between the spatial distribution of rainfall are observed, mainly in region N. The disagreements detected in region N both underestimate and overestimate the distributed rain gauge data. This behaviour suggests a problem due to the sparsity of observed data available to interpolate across region N. The cumulative frequency distribution of the observed gridded data demonstrates that 5% of the cells which represent annual rainfall higher than 3,000 mm show non-normal distributions, strengthening the case that the discrepancies are concentrated in region N (Fig. 5). Similar behaviour was also observed by Tang et al. (2016a) over the Tibetan Plateau, where the sparse gauge network used for the interpolation probably reduced the reliability of metrics calculated against such ground reference. Additionally, we observe that the IMERG-V05 product underestimated the annual rainfall along the NE coastal region. This performance follows the general pattern observed in the daily and monthly analyses when the IMERG-V05 product was not successful in detecting the rainfall events across this area. Additional analyses are necessary in order to assess the possible causes of different performances over Brazil.

INSERT FIG. 5

Fig. 5 Quantile-quantile (Q-Q) plot comparing the cumulative distribution of the IMERG-V05 Final product and ground-based gridded rainfall data. The solid lines represent theoretical normal distributions.

3.2 National-scale evaluation

This evaluation analysed the national comparison between the series from IMERG-V05 and rain gauge grids using the areal means for the entire country. The analysis reveals a strong agreement for the Brazilian territory as a whole, with the satellite data matching the average rainfall records at daily and monthly time scales

(Fig. 6). Generally, the regression line in the scatter plots demonstrates a slight overestimation by the IMERG-V05 product at daily and monthly time scales. Analogous performance analysing the mean areal precipitation was also noticed in others national-scale studies (e.g. Caracciolo et al., 2018; Mayor et al., 2017; Tan and Duan, 2017; Tang et al., 2016a). The national CC at daily and monthly temporal resolutions were 0.96 and 0.99, respectively. These values of the agreement are higher than those from the analysis of the daily and monthly average of individual cells (0.68 and 0.96, respectively). This shows that the areal aggregation leads to an improvement of the satellite product, indicating a good efficacy of the IMERG-V05 product to estimate precipitation over large areas.

INSERT FIG. 6

Fig. 6 Scatter plots and metrics of rainfall comparisons for national-scale evaluation over Brazil at (a) daily and (b) monthly timescales.

Comparisons between ground-based and IMERG-V05 data at national scale show the low variability of ME and RMSE at daily (0.09 and 0.78 mm, respectively) and monthly (2.7 and 6.4 mm, respectively) time scales. The annual average rainfall at national-scale estimated by the IMERG-V05 product for 2016 was 1,647 mm, while the average rainfall of the interpolated data for the same year was 1,615 mm.

3.3 Subarea evaluation

Fig. 7 shows the scatter plots and evaluation metrics based on the mean areal rainfall for the five selected subareas. Each subarea was individually analysed in order to expose the problem related to the low density of gauges used for the interpolation in some regions. Also, this analysis provides more detail on the error characteristics of the IMERG-V05 product. Thus, subareas with a relatively high density of ground-based points were carefully chosen. At the daily time scale, the analysis indicates that the IMERG-V05 product presented a very good agreement for all subareas, with CC ranging between 0.80 (N) and 0.92 (NE). Similarly, the high values of POD (from 0.71 to 0.89) and CSI (from 0.65 to 0.88) showed satisfactory performance of the IMERG-V05 product in detecting the ground-based rainfall events in the subareas. The FAR presented values close to zero for almost all subareas, indicating low false alarms when regions with high density of in-situ data are considered for the analyses. The exception was noticed in region NE (FAR = 0.23) because that subarea is

placed in a dry zone, where there are fewer events to be correctly detected. Muhammad et al. (2018) also found noted low performance of satellite rainfall detection in the driest regions of Pakistan. In addition, more localised rainfall events in semiarid regions can be missed either by rain gauges or reduced to a very low quantity from averaging up to the satellite grid. Conversely, the subarea located in the region NE presented absolute values of ME and RMSE closer to zero due to the low rainfall depth throughout the year, but representing the highest relative values at daily (32.3 and 196%, respectively) and monthly (32.2 and 47.4%, respectively) temporal scales (see Table S1). Once again, the subarea located in region N exhibited the highest absolute values of ME and RMSE because of the largest number of days with rain and the high annual rainfall depth. Nevertheless, the relative ME and RMSE present similar values when compared to regions S, SE, and CW (see Table S1). Overall, all subareas presented a significant improvement of the metrics at the monthly time scale, with most metrics showing near perfect indices by comparing the areal mean of the interpolated gauge data and the IMERG-V05 product.

INSERT FIG. 7

Fig. 7 Metrics for the subarea analysis at daily (a, c, e, g, and i) and monthly (b, d, f, h, and j) scales based on the mean areal precipitation in the five official geographical regions in Brazil.

3.4 Categorical analysis

A categorical analysis was conducted to determine the direct influence of several factors on the daily agreement between the ground-based gridded rainfall data and the IMERG-V05 product. Fig. 8 shows the CC against the density of gauges (left column) and altitude (right column) categorised by the five regions in Brazil. Because of a large number of cells, the concentration of points was coloured in a normalised scale from zero (red) to one (blue), representing the highest and lowest concentrations, respectively. Overall, we observe that the CC inversely correlates to the density of gauges in regions N and CW of the country, with values ranging from 0.1 to 0.8 in areas with less than 10 gauges per 10,000 km^2. In contrast, the correlations between CC and density of gauges have a tendency to increase from this threshold, with values ranging from 0.6 to 0.8. Meanwhile, regions S and SE presented similar behaviour, with CC mostly higher than 0.6 and reaching 0.9 in some places. However, it is worth highlighting that both regions S and SE present the highest density of gauges used for the interpolation, mostly higher than 10 per 10,000 km^2. These results reinforce the result in Tang et

al. (2018) that the spatiotemporal errors computed by comparing satellite and observed rainfall data increase with the reduction of the gauge density in a grid box approach.

INSERT FIG. 8

Fig. 8 Scatter plots of CC vs gauge density (left column) and altitude (right column) categorised by the five regions in Brazil, where the number of grid boxes at each point on the plot is normalised by the highest number on the plot, and then coloured according to the color bar at the bottom of the figure.

The relation between CC and altitude shows a higher scattering and lower concentration of points with the increasing of elevation. In general, the cells located at altitudes higher than 1,000 m above sea level present considerable improvement of CC, which is more noticeable in regions NE, CW, and SE. This find differs from the study carried out by Anjum et al. (2018) in Pakistan. However, it is similar to the results found by Mayor et al. (2017) in a Mexican region, where IMERG performed better at higher altitudes. It is also noticeable that the correlations between CC and altitude in both regions S and SE showed analogous behaviour to those observed for the station density analysis, with small ranges of CC variation according to the elevation. Unlike these two regions, larger dispersions are observed in regions N, NE, and CW for a wide range of elevations. Therefore, the similar behaviour of the scatter plots for both categorical analyses may suggest that the density of gauges affects the altitude evaluation.

In general, the correlation showed that the IMERG-V05 performed better in regions under Subtropical (Zone C) and Semiarid (Zone B) climates (Fig. 9). The Subtropical climate is found mostly in the regions S and SE; whereas the Semiarid climate prevails in NE Brazil. Three climates (Cwc, Csa, and Csb) were excluded from the analysis because they cover less than 0.01% of the Brazilian territory (Alvares et al., 2013). Overall, the climates identified as being part of climatic Zone A (Tropical climate) exhibited the largest dispersions, as well as the lowest means and medians of CC values. Zone A represents the largest climate area in Brazil and covers predominantly regions N and CW. Consequently, the categorical analysis by climate may have been once again influenced by the low density of rain gauges, which probably results in a poor performance of the IMERG-V05 estimates.

INSERT FIG. 9

Fig. 9 Box plots of CC categorised by climate.

4. Conclusions

This study evaluated the IMERG-V05 Final Run product over Brazil using ground-based gridded rainfall data composed of 4,911 gauges as a reference. All analyses were performed in a distributed fashion at daily, monthly, and annual timescales for 2016. Overall, the results showed that the IMERG-V05 product can effectively capture the spatial patterns of rainfall across Brazil. The main specific findings of this study using a grid box-scale approach are summarised as follows:

(1) IMERG-V05 exhibited better agreement with the observed data at monthly timescale when compared to daily timescale in all analyses. Nevertheless, the IMERG-V05 presented a slight tendency in overestimating the gridded observed data at all analysed timescales.

(2) The performance of IMERG-V05 in the grid-scale and national-scale evaluations presented some variations as a function of the analysed region. Based on these two evaluations, the rainfall estimated by the satellite product exhibited higher errors and biases in regions N and CW, as well as along the Atlantic coast of region NE. The underestimation evident in the satellite product for the region NE is likely associated with topographic forcing that favours warm-rain process systems which cannot be detected very well by passive microwave sensors over land.

(3) The subarea evaluation revealed that the IMERG-V05 product compares well with the interpolated data in specific areas with high density of rain gauges, including region N. The categorical analysis confirmed that the low density of rain gauges in regions N and CW can be a source of large deviations, errors, and biases in the evaluation of the satellite rainfall product.

Based on the findings of this study, the IMERG-V05 Final Run product can be used as a source of rainfall data to complement the ground precipitation measurements in most parts of the Brazilian territory. The exception is in the coastal region of the Brazilian NE, where the IMERG-V05 product needs a bias correction procedure due to the large underestimation probably caused by the inability of the microwave and infrared sensors in to properly detect rain-warm events. Moreover, the IMERG-V05 estimates for regions N and CW need to be carefully used because of some uncertainties in the data which are probably associated with the low density of rain gauges used to create the ground-based gridded product.

Finally, this study highlights that the relatively high spatiotemporal resolution of the IMERG-V05 product can favour its application for many purposes in Brazil such as hydrological modelling. However, further

improvements of the IMERG-V05 product are needed for providing more accurate rainfall estimates mainly along the coastal zone of NE Brazil. Furthermore, studies exploring the characteristics of hourly and half-hourly estimates of the IMERG-V05 product over Brazil are strongly recommended.

Acknowledgements: The authors would like to acknowledge the financial support from FINEP (Brazilian Innovation Agency) granted to the BRAMAR (BRAzil Managed Aquifer Recharge, grant no. 557/2013) project. The Brazilian authors are grateful to the Brazilian National Council for Scientific and Technological Development (CNPq), Coordination for the Improvement of Higher Education and Personal (CAPES), Paraíba Research Foundation (FAPESQ-PB), and São Paulo Research Foundation (FAPESP, process 2016/23546-7) for the financial support. The NASA authors (GHJ and WAP) were funded under the Precipitation Measurement Missions and Global Precipitation Measurement (GPM) mission projects. Special thanks are given to ANA (Brazilian National Water Agency), INMET (the Brazilian National Institute of Meteorology), and the sixteen Brazilian regional water agencies (specially ADASA, CAESB, DAEE, FUNCEME, and AGUASPARANÁ) for providing the ground-based rainfall data.

References

Alvares, C.A., Stape, J.L., Sentelhas, P.C., De Moraes Gonçalves, J.L., Sparovek, G., 2013. Köppen's climate classification map for Brazil. Meteorol. Zeitschrift 22, 711–728. doi:10.1127/0941-2948/2013/0507

Anjum, M.N., Ding, Y., Shangguan, D., Ahmad, I., Ijaz, M.W., Farid, H.U., Yagoub, Y.E., Zaman, M., Adnan, M., 2018. Performance evaluation of latest integrated multi-satellite retrievals for Global Precipitation Measurement (IMERG) over the northern highlands of Pakistan. Atmos. Res. 205, 134–146. doi:10.1016/j.atmosres.2018.02.010

Asong, Z.E., Razavi, S., Wheater, H.S., Wong, J.S., 2017. Evaluation of Integrated Multisatellite Retrievals for GPM (IMERG) over Southern Canada against Ground Precipitation Observations: A Preliminary Assessment. J. Hydrometeorol. 18, 1033–1050. doi:10.1175/JHM-D-16-0187.1

Baik, J., Choi, M., 2015. Spatio-temporal variability of remotely sensed precipitation data from COMS and TRMM: Case study of Korean peninsula in East Asia. Adv. Sp. Res. 56, 1125–1138. doi:10.1016/j.asr.2015.06.015

Beria, H., Nanda, T., Bisht, D.S., Chatterjee, C., 2017. Does the GPM mission improve the systematic error component in satellite rainfall estimates over TRMM? An evaluation at a pan-India scale. Hydrol. Earth Syst. Sci. 21, 6117–6134. doi:10.5194/hess-21-6117-2017

Buarque, D.C., De Paiva, R.C.D., Clarke, R.T., Mendes, C.A.B., 2011. A comparison of Amazon rainfall characteristics derived from TRMM, CMORPH and the Brazilian national rain gauge network. J. Geophys. Res. Atmos. 116, 1–12. doi:10.1029/2011JD016060

Caracciolo, D., Francipane, A., Francesco, V., Noto, L.V., 2018. Performances of GPM satellite precipitation over the two major Mediterranean islands CLIMB -Climate Induces Changes on the Hydrology of Mediterranean Basins View project CLIMB FP7 View project. Atmos. Res. 213, 309–322. doi:10.1016/j.atmosres.2018.06.010

Coelho, V.H.R., Montenegro, S., Almeida, C.N., Silva, B.B., Oliveira, L.M., Gusmão, A.C. V, Freitas, E.S., Montenegro, A.A.A., 2017. Alluvial groundwater recharge estimation in semi-arid environment using remotely sensed data. J. Hydrol. 548, 1–15. doi:10.1016/j.jhydrol.2017.02.054

Cohen Liechti, T., Matos, J.P., Boillat, J.L., Schleiss, A.J., 2012. Comparison and evaluation of satellite derived precipitation products for hydrological modeling of the Zambezi River Basin. Hydrol. Earth Syst. Sci. 16, 489–500. doi:10.5194/hess-16-489-2012

Collischonn, B., Collischonn, W., Tucci, C.E.M., 2008. Daily hydrological modeling in the Amazon basin using TRMM rainfall estimates. J. Hydrol. 360, 207–216. doi:10.1016/j.jhydrol.2008.07.032

Curtarelli, M.P., Rennó, C.D., Alcântara, E.H., 2014. Evaluation of the Tropical Rainfall Measuring Mission 3B43 product over an inland area in Brazil and the effects of satellite boost on rainfall estimates. J. Appl. Remote Sens. 8, 083589. doi:10.1117/1.JRS.8.083589

De Paiva, R.C.D., Buarque, D.C., Collischonn, W., Bonnet, M.P., Frappart, F., Calmant, S., Bulhões Mendes, C.A., 2013. Large-scale hydrologic and hydrodynamic modeling of the Amazon River basin. Water Resour. Res. 49, 1226–1243. doi:10.1002/wrcr.20067

Delahaye, F., Kirstetter, P.E., Dubreuil, V., Machado, L.A.T., Vila, D.A., Clark, R., 2015. A consistent gauge database for daily rainfall analysis over the Legal Brazilian Amazon. J. Hydrol. 527, 292–304. doi:10.1016/j.jhydrol.2015.04.012

Dezfuli, A.K., Ichoku, C.M., Huffman, G.J., Mohr, K.I., Selker, J.S., van de Giesen, N., Hochreutener, R., Annor, F.O., 2017. Validation of IMERG precipitation in Africa. J. Hydrometeorol. JHM-D-17-0139.1. doi:10.1175/JHM-D-17-0139.1

Espinoza Villar, J.C., Ronchail, J., Guyot, J.L., Cochonneau, G., Naziano, F., Lavado, W., De Oliveira, E., Pombosa, R., Vauchel, P., 2009. Spatio-temporal rainfall variability in the Amazon basin countries (Brazil, Peru, Bolivia, Colombia, and Ecuador). Int. J. Climatol. 29, 1574–1594. doi:10.1002/joc.1791

Falck, A.S., Maggioni, V., Tomasella, J., Vila, D.A., Diniz, F.L.R., 2015. Propagation of satellite precipitation uncertainties through a distributed hydrologic model: A case study in the Tocantins-Araguaia basin in Brazil. J. Hydrol. 527, 943–957. doi:10.1016/j.jhydrol.2015.05.042

Fang, J., Du, J., Xu, W., Shi, P., Li, M., Ming, X., 2013. Spatial downscaling of TRMM precipitation data based on the orographical effect and meteorological conditions in a mountainous area. Adv. Water Resour. 61, 42–50. doi:10.1016/j.advwatres.2013.08.011

Gebregiorgis, A.S., Kirstetter, P.E., Hong, Y.E., Gourley, J.J., Huffman, G.J., Petersen, W.A., Xue, X., Schwaller, M.R., 2018. To What Extent is the Day 1 GPM IMERG Satellite Precipitation Estimate Improved as Compared to TRMM TMPA-RT? J. Geophys. Res. Atmos. 123, 1694–1707. doi:10.1002/2017JD027606

Guo, R., Liu, Y., 2016. Evaluation of satellite precipitation products with rain gauge data at different scales: Implications for hydrological applications. Water (Switzerland) 8. doi:10.3390/w8070281

Hobouchian, M.P., Salio, P., García Skabar, Y., Vila, D., Garreaud, R., 2017. Assessment of satellite precipitation estimates over the slopes of the subtropical Andes. Atmos. Res. 190, 43–54. doi:10.1016/j.atmosres.2017.02.006

Hofstra, N., New, M., 2009. Spatial variability in correlation decay distance and influence on angular-distance weighting interpolation of daily precipitation over Europe. Int. J. Climatol. 29, 1872–1880. doi:10.1002/joc.1819

Hou, A.Y., Kakar, R.K., Neeck, S., Azarbarzin, A.A., Kummerow, C.D., Kojima, M., Oki, R., Nakamura, K., Iguchi, T., 2014. The global precipitation measurement mission. Bull. Am. Meteorol. Soc. 95, 701–722. doi:10.1175/BAMS-D-13-00164.1

Huffman, G.J., Bolvin, D.T., Nelkin, E.J., 2017a. Integrated Multi-satellitE Retrievals for GPM (IMERG) Technical Documentation.

Huffman, G.J., Bolvin, D.T., Nelkin, E.J., Stocker, E.F., 2017b. V05 IMERG Final Run Release Notes.

Huffman, G.J., Bolvin, D.T., Nelkin, E.J., Wolff, D.B., Adler, R.F., Gu, G., Hong, Y., Bowman, K.P., Stocker, E.F., 2007. The TRMM Multisatellite Precipitation Analysis (TMPA): Quasi-Global, Multiyear, Combined-Sensor Precipitation Estimates at Fine Scales. J. Hydrometeorol. 8, 38–55. doi:10.1175/JHM560.1

Jesus, M., Rinaldo, A., Rodr, I., Jesus, D.E.L., Al, E.T., 2015. Point rainfall statistics for ecohydrological analyses derived from satellite integrated measurements. Water Resour. Res. 2974–2985. doi:10.1002/2015WR016935.Received

Kann, A., Meirold-Mautner, I., Schmid, F., Kirchengast, G., Fuchsberger, J., Meyer, V., Tüchler, L., Bica, B., 2015. Evaluation of high-resolution precipitation analyses using a dense station network. Hydrol. Earth Syst. Sci. 19, 1547–1559. doi:10.5194/hess-19-1547-2015

Kidd, C., Becker, A., Huffman, G.J., Muller, C.L., Joe, P., Skofronick-Jackson, G., Kirschbaum, D.B., 2017. So, how much of the Earth's surface is covered by rain gauges? Bull. Am. Meteorol. Soc. 98, 69–78. doi:10.1175/BAMS-D-14-00283.1

Kidd, C., Huffman, G., 2011. Global precipitation measurement. Meteorol. Appl. 18, 334–353. doi:10.1002/met.284

Kousky, V.E., 1979. Frontal Influences on Northeast Brazil. Mon. Weather Rev. doi:10.1175/1520-0493(1979)107<1140:FIONB>2.0.CO;2

Lelis, L., Bosquilia, R., Duarte, S., 2018. Assessment of Precipitation Data Generated by GPM and TRMM Satellites. Rev. Bras. Meteorol. 33, 153–163. doi:http://dx.doi.org/10.1590/0102-7786331004 rbmet.org.br Artigo

553 Levizzani, V., Kidd, C., Aonashi, K., Bennartz, R., Ferraro, R.R., Huffman, G.J., Roca, R., Turk, F.J., Wang, N.Y., 2018.
554 The activities of the International Precipitation Working Group. Q. J. R. Meteorol. Soc. doi:10.1002/qj.3214
555 Liu, Z., Ostrenga, D., Vollmer, B., Deshong, B., MacRitchie, K., Greene, M., Kempler, S., 2017. Global precipitation
556 measurement mission products and services at the nasa ges disc. Bull. Am. Meteorol. Soc. 98, 437–444.
557 doi:10.1175/BAMS-D-16-0023.1
558 Mahmoud, M.T., Al-zahrani, M.A., Sharif, H.O., 2018. Assessment of global precipitation measurement satellite products
559 over Saudi Arabia. J. Hydrol. 559, 1–12. doi:10.1016/j.jhydrol.2018.02.015
560 Mayor, Y.G., Tereshchenko, I., Fonseca-Hernández, M., Pantoja, D.A., Montes, J.M., 2017. Evaluation of error in IMERG
561 precipitation estimates under different topographic conditions and temporal scales over Mexico. Remote Sens. 9.
562 doi:10.3390/rs9050503
563 McMillan, H., Jackson, B., Clark, M., Kavetski, D., Woods, R., 2011. Rainfall uncertainty in hydrological modelling: An
564 evaluation of multiplicative error models. J. Hydrol. 400, 83–94. doi:10.1016/j.jhydrol.2011.01.026
565 Melo, D.C.D., Xavier, A.C., Bianchi, T., Oliveira, P.T.S., Scanlon, B.R., Lucas, M.C., Wendland, E., 2015. Performance
566 evaluation of rainfall estimates by TRMM Multi-satellite Precipitation Analysis 3B42V6 and V7 over Brazil. J.
567 Geophys. Res. Atmos. 120, 9043–9836. doi:10.1002/2014JD022963
568 Melo, D.D.C.D., Scanlon, B.R., Zhang, Z., Wendland, E., Yin, L., 2016. Reservoir storage and hydrologic responses to
569 droughts in the Paraná River basin, south-eastern Brazil 4673–4688. doi:10.5194/hess-20-4673-2016
570 Meng, J., Li, L., Hao, Z., Wang, J., Shao, Q., 2014. Suitability of TRMM satellite rainfall in driving a distributed
571 hydrological model in the source region of Yellow River. J. Hydrol. 509, 320–332. doi:10.1016/j.jhydrol.2013.11.049
572 Mitra, A.K., Kaushik, N., Singh, A.K., Parihar, S., Bhan, S.C., 2018. Evaluation of INSAT-3D Satellite derived precipitation
573 estimates for Heavy Rainfall Events and its Validation with Gridded GPM (IMERG) rainfall Dataset over the Indian
574 region Remote Sensing Applications : Society and Environment Evaluation of INSAT-3D s. Remote Sens. Appl.
575 Soc. Environ. 9, 91–99. doi:10.1016/j.rsase.2017.12.006
576 Muhammad, W., Yang, H., Lei, H., Muhammad, A., Yang, D., 2018. Improving the regional applicability of satellite
577 precipitation products by ensemble algorithm. Remote Sens. 10, 577. doi:10.3390/rs10040577
578 Naumann, G., Barbosa, P., Carrao, H., Singleton, A., Vogt, J., 2012. Monitoring drought conditions and their uncertainties
579 in Africa using TRMM data. J. Appl. Meteorol. Climatol. 51, 1867–1874. doi:10.1175/JAMC-D-12-0113.1
580 Nery, J.T., Carfan, A.C., 2014. Re-analysis of pluvial precipitation in southern Brazil. Atmosfera 27, 103–115.
581 doi:10.1016/S0187-6236(14)71104-X
582 New, M., Hulme, M., Jones, P., 2000. Representing twentieth-century space-time climate variability. Part II: Development
583 of 1901-96 monthly grids of terrestrial surface climate. J. Clim. 13, 2217–2238. doi:10.1175/1520-

584 0442(2000)013<2217:RTCSTC>2.0.CO;2
585 O, S., Kirstetter, P.E., 2018. Evaluation of diurnal variation of GPM IMERG-derived summer precipitation over the
586 contiguous US using MRMS data. Q. J. R. Meteorol. Soc. doi:10.1002/qj.3218
587 Oliveira, R., Maggioni, V., Vila, D., Morales, C., 2016. Characteristics and diurnal cycle of GPM rainfall estimates over
588 the Central Amazon region. Remote Sens. 8. doi:10.3390/rs8070544
589 Oliveira, R., Maggioni, V., Vila, D., Porcacchia, L., 2018. Using satellite error modeling to improve GPM-Level 3 rainfall
590 estimates over the central Amazon region. Remote Sens. 10. doi:10.3390/rs10020336
591 Palharini, R.S.A., Vila, D.A., 2017. Climatological behavior of precipitating clouds in the northeast region of Brazil. Adv.
592 Meteorol. 17–21.
593 Pombo, S., de Oliveira, R.P., 2015. Evaluation of extreme precipitation estimates from TRMM in Angola. J. Hydrol. 523,
594 663–679. doi:10.1016/j.jhydrol.2015.02.014
595 Prakash, S., Mitra, A.K., Aghakouchak, A., Liu, Z., Norouzi, H., Pai, D.S., 2018. A preliminary assessment of GPM-based
596 multi-satellite precipitation estimates over a monsoon dominated region. J. Hydrol. 556, 865–876.
597 doi:10.1016/j.jhydrol.2016.01.029
598 Prakash, S., Mitra, A.K., Pai, D.S., Aghakouchak, A., 2016. Advances in Water Resources From TRMM to GPM : How
599 well can heavy rainfall be detected from space ? Adv. Water Resour. 88, 1–7. doi:10.1016/j.advwatres.2015.11.008
600 Rozante, J.R. and, Vila, D.A. and, Chiquetto, Júlio Barboza and Fernandes, A. de A. and, Alvim, D.S., 2018. Evaluation of
601 TRMM/GPM Blended Daily Products over Brazil. Remote Sens. 15, 814–815.
602 doi:https://doi.org/10.3390/rs10060882
603 Satgé, F., Xavier, A., Zolá, R.P., Hussain, Y., Timouk, F., Garnier, J., Bonnet, M.P., 2017. Comparative assessments of the
604 latest GPM mission's spatially enhanced satellite rainfall products over the main bolivian watersheds. Remote Sens.
605 9, 1–16. doi:10.3390/rs9040369
606 Schneider, U., Ziese, M., Meyer-Christoffer, A., Finger, P., Rustemeier, E., Becker, A., 2016. The new portfolio of global
607 precipitation data products of the Global Precipitation Climatology Centre suitable to assess and quantify the global
608 water cycle and resources. Proc. Int. Assoc. Hydrol. Sci. 374, 29–34. doi:10.5194/piahs-374-29-2016
609 Skofronick-Jackson, G., Kirschbaum, D., Petersen, W., Huffman, G., Kidd, C., Stocker, E., Kakar, R., 2018. The Global
610 Precipitation Measurement (GPM) mission's scientific achievements and societal contributions: reviewing four years
611 of advanced rain and snow observations. Q. J. R. Meteorol. Soc. doi:10.1002/qj.3313
612 Skofronick-Jackson, G., Petersen, W.A., Berg, W., Kidd, C., Stocker, E.F., Kirschbaum, D.B., Kakar, R., Braun, S.A.,
613 Huffman, G.J., Iguchi, T., Kirstetter, P.E., Kummerow, C., Meneghini, R., Oki, R., Olson, W.S., Takayabu, Y.N.,
614 Furukawa, K., Wilheit, T., 2017. The global precipitation measurement (GPM) mission for science and Society. Bull.

615 Am. Meteorol. Soc. 98, 1679–1695. doi:10.1175/BAMS-D-15-00306.1
616 Sungmin, O., Foelsche, U., Kirchengast, G., Fuchsberger, J., Tan, J., Petersen, W.A., 2017. Evaluation of GPM IMERG
617 Early, Late, and Final rainfall estimates using WegenerNet gauge data in southeastern Austria. Hydrol. Earth Syst.
618 Sci. 21, 6559–6572. doi:10.5194/hess-21-6559-2017
619 Tan, J., Petersen, W.A., Kirstetter, P.-E., Tian, Y., 2017. Performance of IMERG as a Function of Spatiotemporal Scale. J.
620 Hydrometeorol. 18, 307–319. doi:10.1175/JHM-D-16-0174.1
621 Tan, M., Duan, Z., 2017. Assessment of GPM and TRMM Precipitation Products over Singapore. Remote Sens. 9, 720.
622 doi:10.3390/rs9070720
623 Tan, M.L., Santo, H., 2018. Comparison of GPM IMERG, TMPA 3B42 and PERSIANN-CDR satellite precipitation
624 products over Malaysia. Atmos. Res. 202, 63–76. doi:10.1016/j.atmosres.2017.11.006
625 Tang, G., Behrangi, A., Long, D., Li, C., Hong, Y., 2018. Accounting for spatiotemporal errors of gauges: A critical step to
626 evaluate gridded precipitation products. J. Hydrol. 559, 294–306. doi:10.1016/j.jhydrol.2018.02.057
627 Tang, G., Ma, Y., Long, D., Zhong, L., Hong, Y., 2016a. Evaluation of GPM Day-1 IMERG and TMPA Version-7 legacy
628 products over Mainland China at multiple spatiotemporal scales. J. Hydrol. 533, 152–167.
629 doi:10.1016/j.jhydrol.2015.12.008
630 Tang, G., Zeng, Z., Long, D., Guo, X., Yong, B., Zhang, W., Hong, Y., 2016b. Statistical and Hydrological Comparisons
631 between TRMM and GPM Level-3 Products over a Midlatitude Basin: Is Day-1 IMERG a Good Successor for TMPA
632 3B42V7? J. Hydrometeorol. 17, 121–137. doi:10.1175/JHM-D-15-0059.1
633 Terink, W., Leijnse, H., van den Eertwegh, G., Uijlenhoet, R., 2018. Spatial resolutions in areal rainfall estimation and their
634 impact on hydrological simulations of a lowland catchment. J. Hydrol. doi:10.1016/j.jhydrol.2018.05.045
635 Toté, C., Patricio, D., Boogaard, H., van der Wijngaart, R., Tarnavsky, E., Funk, C., 2015. Evaluation of satellite rainfall
636 estimates for drought and flood monitoring in Mozambique. Remote Sens. 7, 1758–1776. doi:10.3390/rs70201758
637 Wang, Z., Zhong, R., Lai, C., Chen, J., 2017. Evaluation of the GPM IMERG satellite-based precipitation products and the
638 hydrological utility. Atmos. Res. 196, 151–163. doi:10.1016/j.atmosres.2017.06.020
639 WMO, 1994. Guide to hydrological practices: Data acquisition and processing, analysis, forecasting and other applications.
640 Xavier, A.C., King, C.W., Scanlon, B.R., 2016. Daily gridded meteorological variables in Brazil (1980-2013). Int. J.
641 Climatol. 2659, 2644–2659. doi:10.1002/joc.4518
642 Yang, S., Nesbitt, S.W., 2014. Statistical properties of precipitation as observed by the TRMM precipitation radar. Geophys.
643 Res. Lett. 41, 5636–5643. doi:10.1002/2014GL060683
644 Zad, S.N.M., Zulkafli, Z., Muharram, F.M., 2018. Satellite rainfall (TRMM 3B42-V7) performance assessment and
645 adjustment over Pahang river basin, Malaysia. Remote Sens. 10, 1–24. doi:10.3390/rs10030388

646 Zhang, S., Wang, D., Qin, Z., Zheng, Y., Guo, J., 2018. Assessment of the GPM and TRMM Precipitation Products Using
647 the Rain Gauge Network over the Tibetan Plateau. J. Meteorol. Res. 32, 324–336. doi:10.1007/s13351-018-7067-0
648

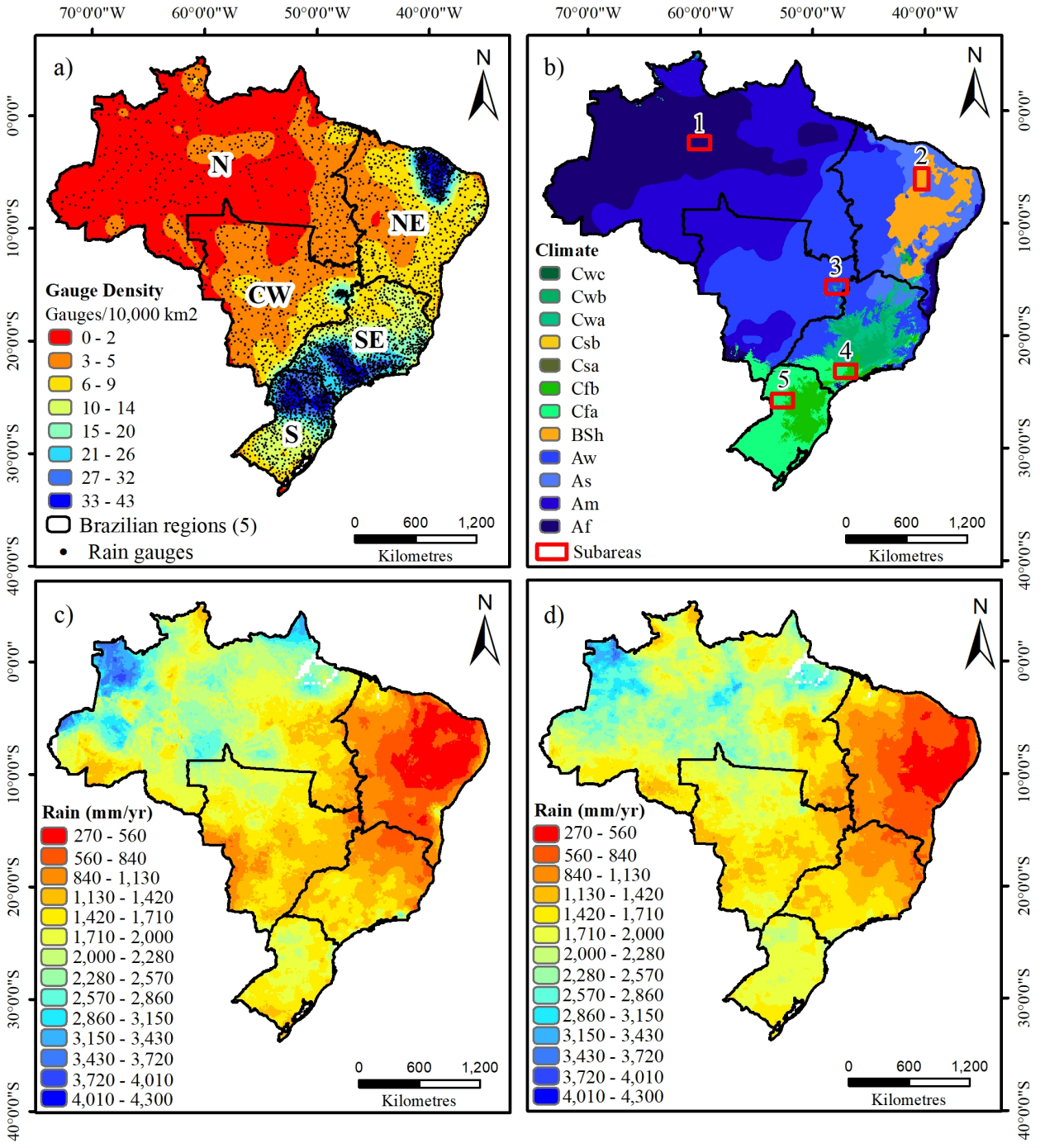
70°0'0"W
60°0'0"W
50°0'0"W
40°0'0"W
0°0'0"
10°0'0"S
20°0'0"S
30°0'0"S
40°0'0"S
a)
N
NE
CW
SE
S
Gauge Density
Gauges/10,000 km2
0 - 2
3 - 5
6 - 9
10 - 14
15 - 20
21 - 26
27 - 32
33 - 43
Brazilian regions (5)
Rain gauges
0
600
1,200
Kilometres
b)
1
2
3
4
5
Climate
Cwc
Cwb
Cwa
Csb
Csa
Cfb
Cfa
BSh
Aw
As
Am
Af
Subareas
c)
Rain (mm/yr)
270 - 560
560 - 840
840 - 1,130
1,130 - 1,420
1,420 - 1,710
1,710 - 2,000
2,000 - 2,280
2,280 - 2,570
2,570 - 2,860
2,860 - 3,150
3,150 - 3,430
3,430 - 3,720
3,720 - 4,010
4,010 - 4,300
d)

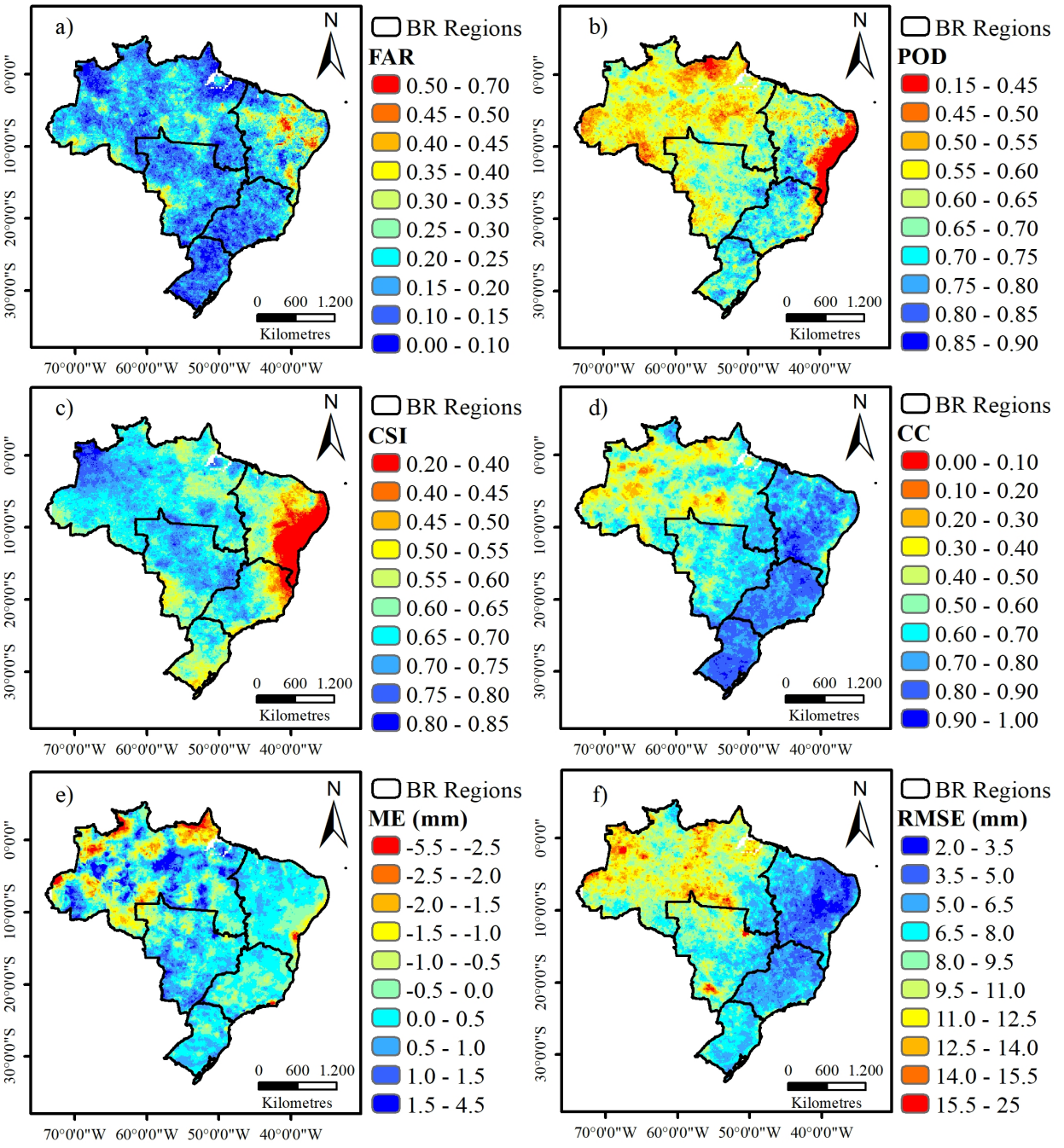
a)
N
BR Regions
FAR
0.50 - 0.70
0.45 - 0.50
0.40 - 0.45
0.35 - 0.40
0.30 - 0.35
0.25 - 0.30
0.20 - 0.25
0.15 - 0.20
0.10 - 0.15
0.00 - 0.10
0 600 1.200
Kilometres
0°0'0"
10°0'0"S
20°0'0"S
30°0'0"S
70°0'0"W 60°0'0"W 50°0'0"W 40°0'0"W
b)
N
BR Regions
POD
0.15 - 0.45
0.45 - 0.50
0.50 - 0.55
0.55 - 0.60
0.60 - 0.65
0.65 - 0.70
0.70 - 0.75
0.75 - 0.80
0.80 - 0.85
0.85 - 0.90
0 600 1.200
Kilometres
0°0'0"
10°0'0"S
20°0'0"S
30°0'0"S
70°0'0"W 60°0'0"W 50°0'0"W 40°0'0"W
c)
N
BR Regions
CSI
0.20 - 0.40
0.40 - 0.45
0.45 - 0.50
0.50 - 0.55
0.55 - 0.60
0.60 - 0.65
0.65 - 0.70
0.70 - 0.75
0.75 - 0.80
0.80 - 0.85
0 600 1.200
Kilometres
0°0'0"
10°0'0"S
20°0'0"S
30°0'0"S
70°0'0"W 60°0'0"W 50°0'0"W 40°0'0"W
d)
N
BR Regions
CC
0.00 - 0.10
0.10 - 0.20
0.20 - 0.30
0.30 - 0.40
0.40 - 0.50
0.50 - 0.60
0.60 - 0.70
0.70 - 0.80
0.80 - 0.90
0.90 - 1.00
0 600 1.200
Kilometres
0°0'0"
10°0'0"S
20°0'0"S
30°0'0"S
70°0'0"W 60°0'0"W 50°0'0"W 40°0'0"W
e)
N
BR Regions
ME (mm)
-5.5 - -2.5
-2.5 - -2.0
-2.0 - -1.5
-1.5 - -1.0
-1.0 - -0.5
-0.5 - 0.0
0.0 - 0.5
0.5 - 1.0
1.0 - 1.5
1.5 - 4.5
0 600 1.200
Kilometres
0°0'0"
10°0'0"S
20°0'0"S
30°0'0"S
70°0'0"W 60°0'0"W 50°0'0"W 40°0'0"W
f)
N
BR Regions
RMSE (mm)
2.0 - 3.5
3.5 - 5.0
5.0 - 6.5
6.5 - 8.0
8.0 - 9.5
9.5 - 11.0
11.0 - 12.5
12.5 - 14.0
14.0 - 15.5
15.5 - 25
0 600 1.200
Kilometres
0°0'0"
10°0'0"S
20°0'0"S
30°0'0"S
70°0'0"W 60°0'0"W 50°0'0"W 40°0'0"W

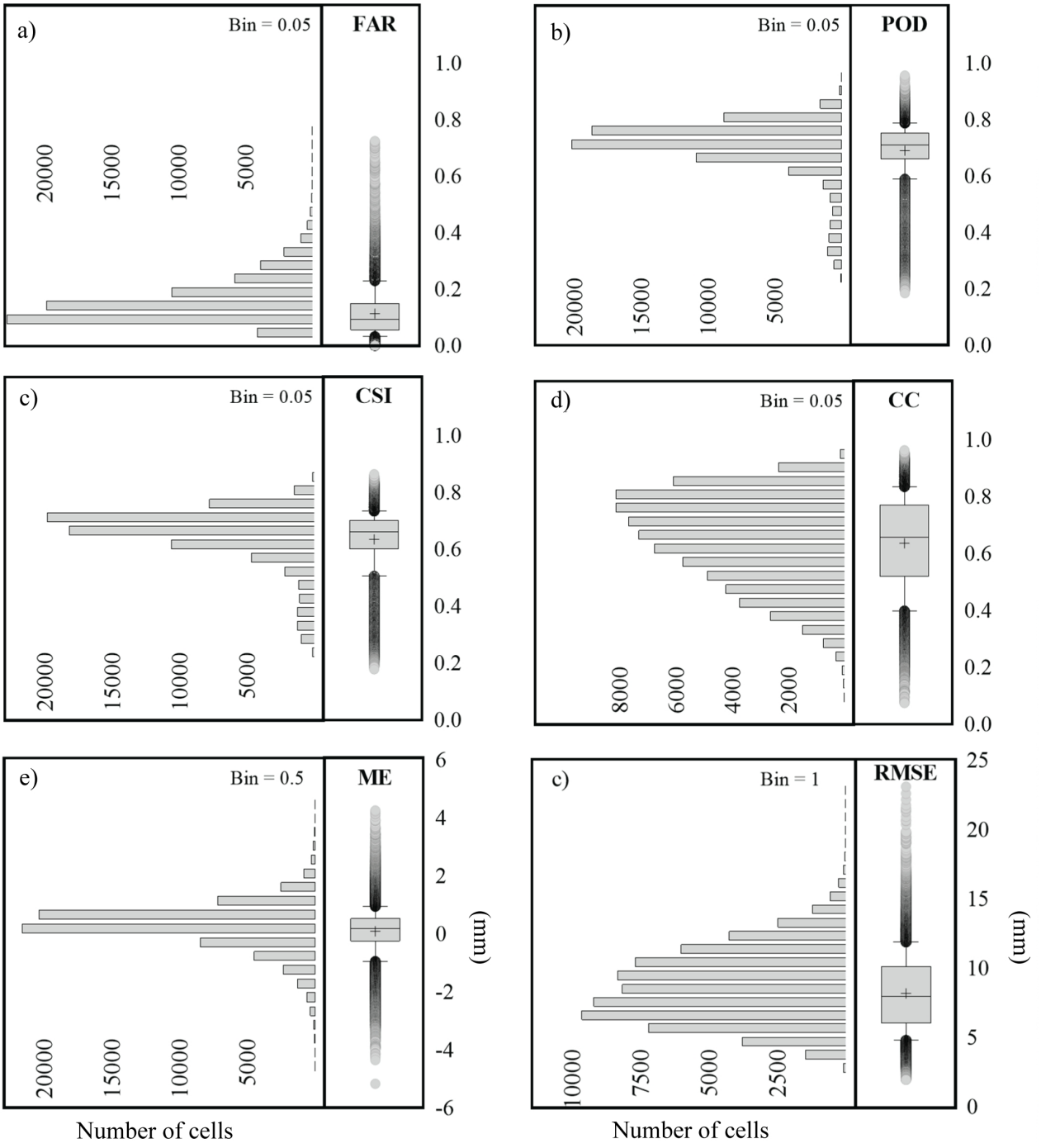
a)
Bin = 0.05
FAR
20000
15000
10000
5000
1.0
0.8
0.6
0.4
0.2
0.0
b)
Bin = 0.05
POD
20000
15000
10000
5000
1.0
0.8
0.6
0.4
0.2
0.0
c)
Bin = 0.05
CSI
20000
15000
10000
5000
1.0
0.8
0.6
0.4
0.2
0.0
d)
Bin = 0.05
CC
8000
6000
4000
2000
1.0
0.8
0.6
0.4
0.2
0.0
e)
Bin = 0.5
ME
20000
15000
10000
5000
6
4
2
0
-2
-4
-6
(mm)
Number of cells
c)
Bin = 1
RMSE
10000
7500
5000
2500
25
20
15
10
5
0
(mm)
Number of cells

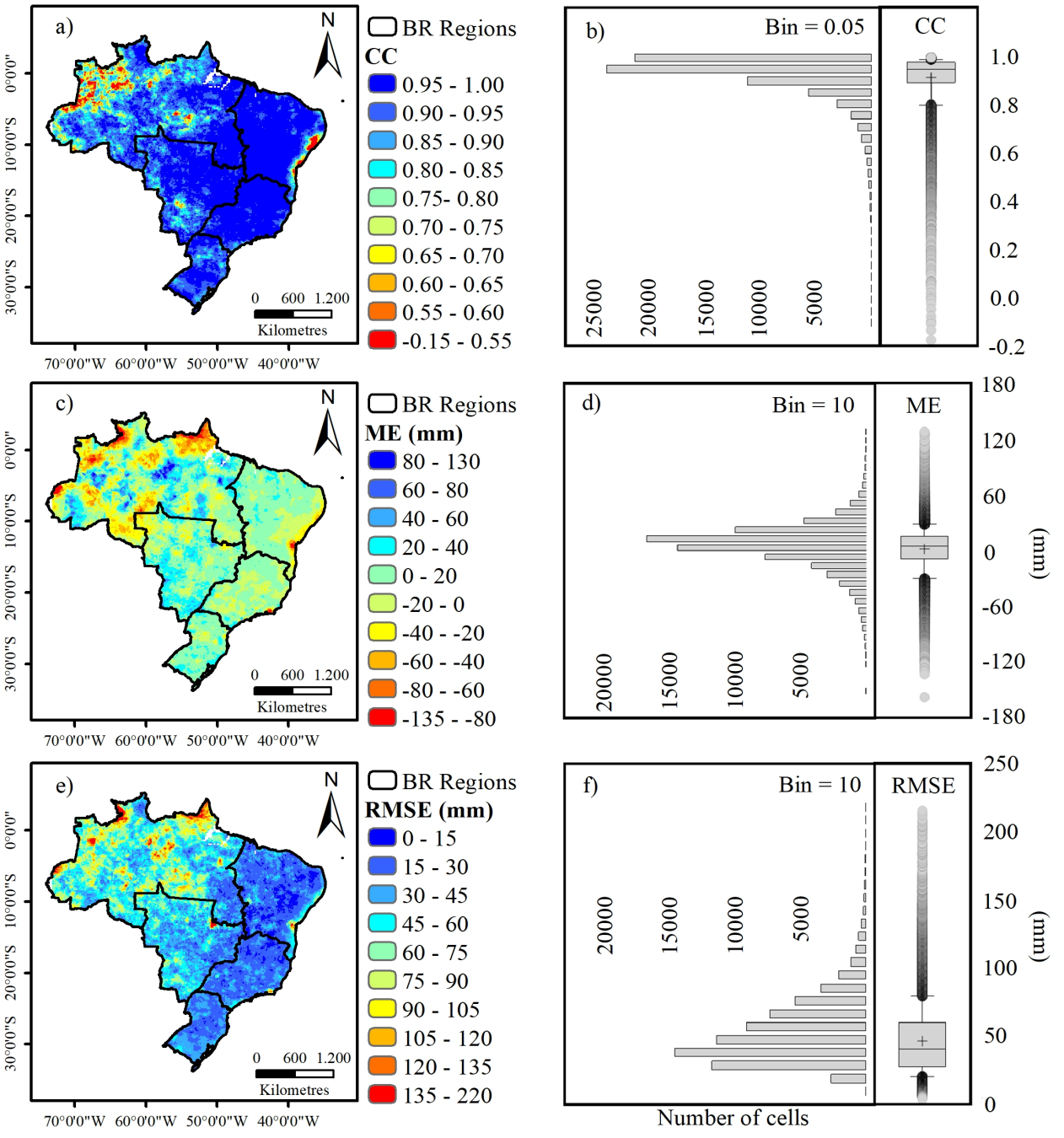
a)
N
BR Regions
CC
0.95 - 1.00
0.90 - 0.95
0.85 - 0.90
0.80 - 0.85
0.75- 0.80
0.70 - 0.75
0.65 - 0.70
0.60 - 0.65
0.55 - 0.60
-0.15 - 0.55
0 600 1.200
Kilometres
0°0'0"
10°0'0"S
20°0'0"S
30°0'0"S
70°0'0"W 60°0'0"W 50°0'0"W 40°0'0"W
b)
Bin = 0.05
CC
25000
20000
15000
10000
5000
1.0
0.8
0.6
0.4
0.2
0.0
-0.2
c)
N
BR Regions
ME (mm)
80 - 130
60 - 80
40 - 60
20 - 40
0 - 20
-20 - 0
-40 - -20
-60 - -40
-80 - -60
-135 - -80
0 600 1.200
Kilometres
0°0'0"
10°0'0"S
20°0'0"S
30°0'0"S
70°0'0"W 60°0'0"W 50°0'0"W 40°0'0"W
d)
Bin = 10
ME
20000
15000
10000
5000
180
120
60
0
-60
-120
-180
(mm)
e)
N
BR Regions
RMSE (mm)
0 - 15
15 - 30
30 - 45
45 - 60
60 - 75
75 - 90
90 - 105
105 - 120
120 - 135
135 - 220
0 600 1.200
Kilometres
0°0'0"
10°0'0"S
20°0'0"S
30°0'0"S
70°0'0"W 60°0'0"W 50°0'0"W 40°0'0"W
f)
Bin = 10
RMSE
20000
15000
10000
5000
250
200
150
100
50
0
(mm)
Number of cells

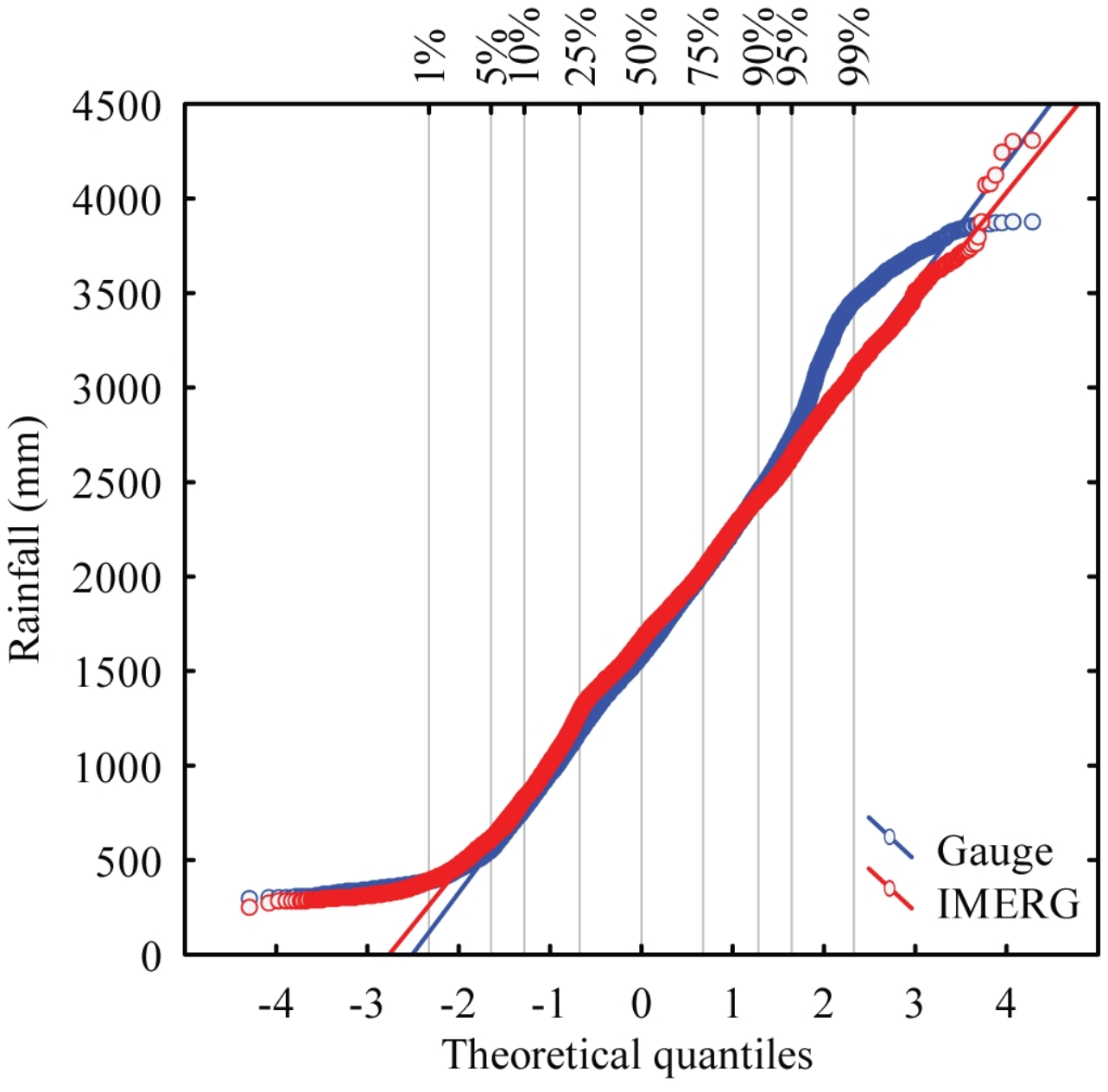
1%
5%
10%
25%
50%
75%
90%
95%
99%
4500
4000
3500
3000
2500
2000
1500
1000
500
0
Rainfall (mm)
-4
-3
-2
-1
0
1
2
3
4
Theoretical quantiles
Gauge
IMERG

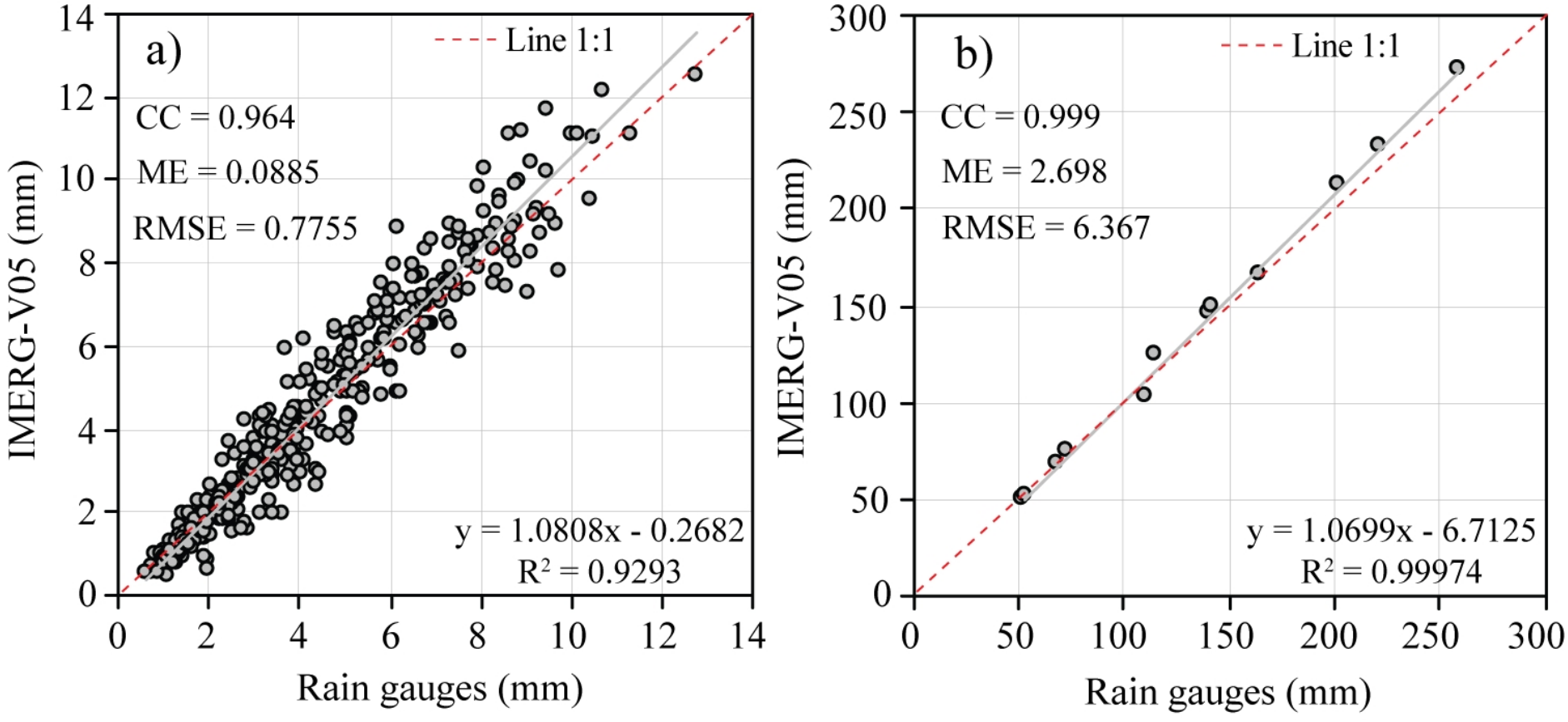
a)
Line 1:1
CC = 0.964
ME = 0.0885
RMSE = 0.7755
y = 1.0808x - 0.2682
R² = 0.9293
IMERG-V05 (mm)
Rain gauges (mm)
0
2
4
6
8
10
12
14
b)
Line 1:1
CC = 0.999
ME = 2.698
RMSE = 6.367
y = 1.0699x - 6.7125
R² = 0.99974
IMERG-V05 (mm)
Rain gauges (mm)
0
50
100
150
200
250
300

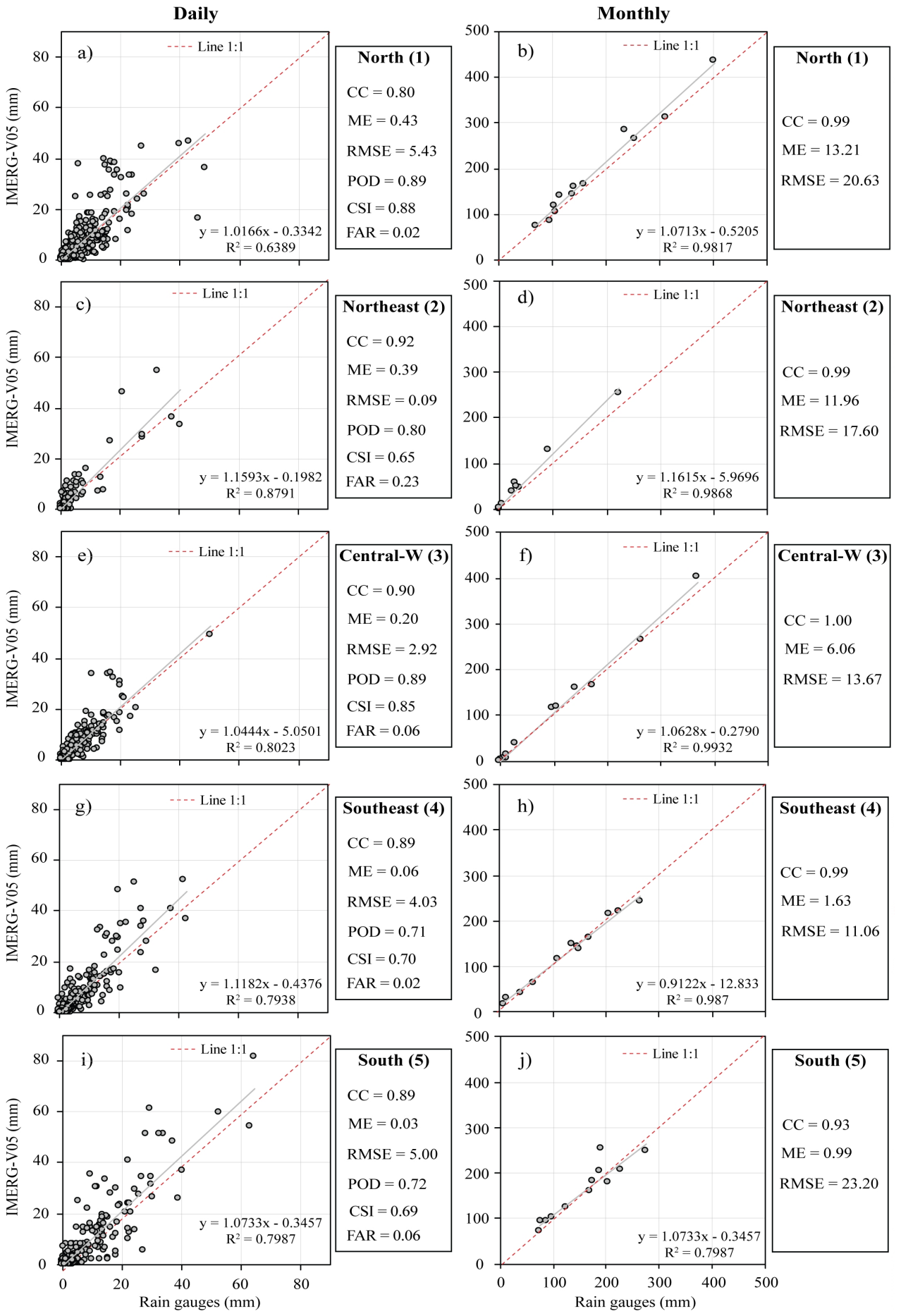
Daily
Monthly
a)
Line 1:1
y = 1.0166x - 0.3342
R² = 0.6389
North (1)
CC = 0.80
ME = 0.43
RMSE = 5.43
POD = 0.89
CSI = 0.88
FAR = 0.02
b)
Line 1:1
y = 1.0713x - 0.5205
R² = 0.9817
North (1)
CC = 0.99
ME = 13.21
RMSE = 20.63
c)
Line 1:1
y = 1.1593x - 0.1982
R² = 0.8791
Northeast (2)
CC = 0.92
ME = 0.39
RMSE = 0.09
POD = 0.80
CSI = 0.65
FAR = 0.23
d)
Line 1:1
y = 1.1615x - 5.9696
R² = 0.9868
Northeast (2)
CC = 0.99
ME = 11.96
RMSE = 17.60
e)
Line 1:1
y = 1.0444x - 5.0501
R² = 0.8023
Central-W (3)
CC = 0.90
ME = 0.20
RMSE = 2.92
POD = 0.89
CSI = 0.85
FAR = 0.06
f)
Line 1:1
y = 1.0628x - 0.2790
R² = 0.9932
Central-W (3)
CC = 1.00
ME = 6.06
RMSE = 13.67
g)
Line 1:1
y = 1.1182x - 0.4376
R² = 0.7938
Southeast (4)
CC = 0.89
ME = 0.06
RMSE = 4.03
POD = 0.71
CSI = 0.70
FAR = 0.02
h)
Line 1:1
y = 0.9122x - 12.833
R² = 0.987
Southeast (4)
CC = 0.99
ME = 1.63
RMSE = 11.06
i)
Line 1:1
y = 1.0733x - 0.3457
R² = 0.7987
South (5)
CC = 0.89
ME = 0.03
RMSE = 5.00
POD = 0.72
CSI = 0.69
FAR = 0.06
j)
Line 1:1
y = 1.0733x - 0.3457
R² = 0.7987
South (5)
CC = 0.93
ME = 0.99
RMSE = 23.20
IMERG-V05 (mm)
Rain gauges (mm)
0
20
40
60
80
100
200
300
400
500

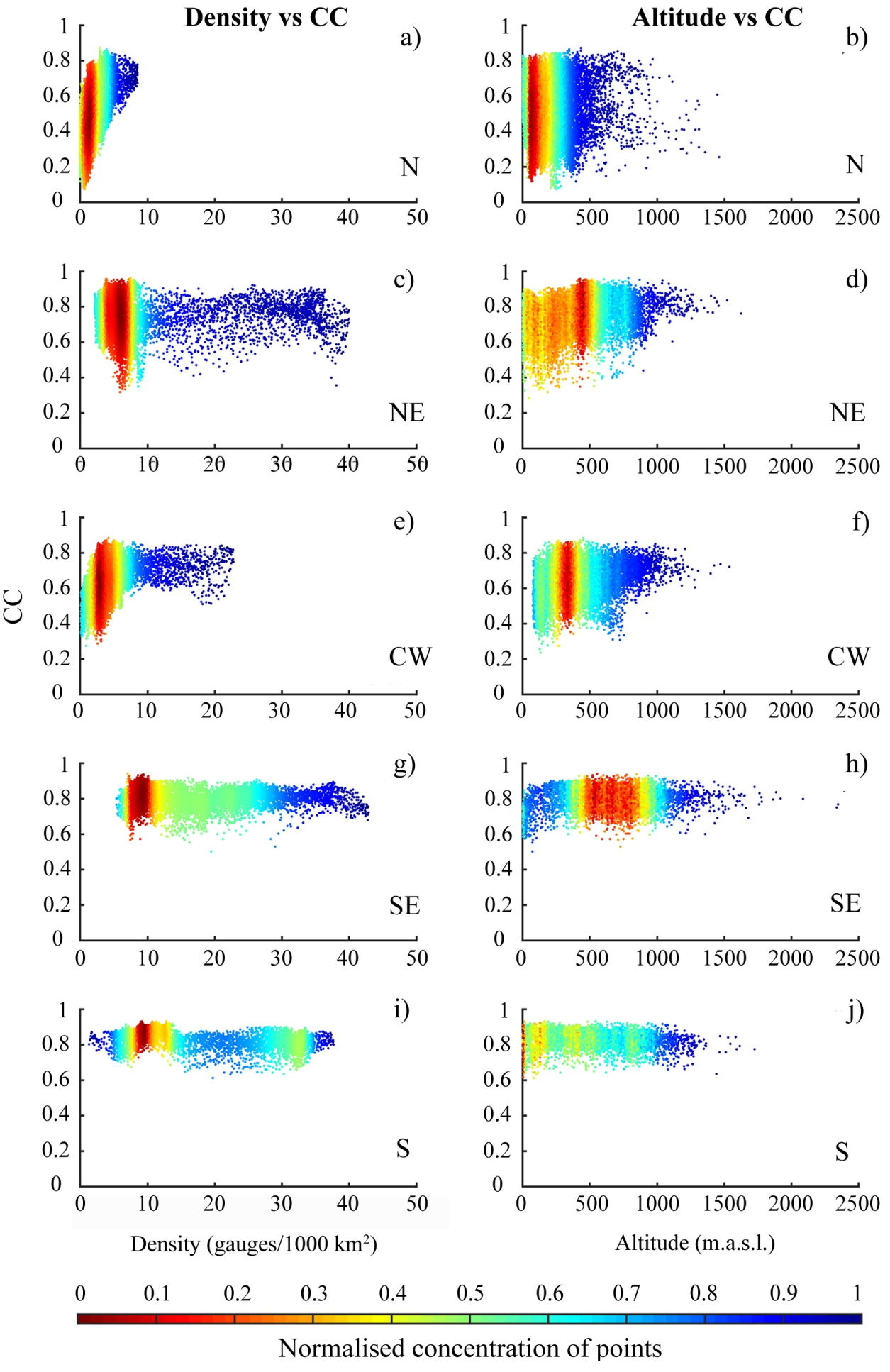
Density vs CC
Altitude vs CC
a)
b)
c)
d)
e)
f)
g)
h)
i)
j)
N
NE
CW
SE
S
CC
Density (gauges/1000 km²)
Altitude (m.a.s.l.)
0 0.1 0.2 0.3 0.4 0.5 0.6 0.7 0.8 0.9 1
Normalised concentration of points

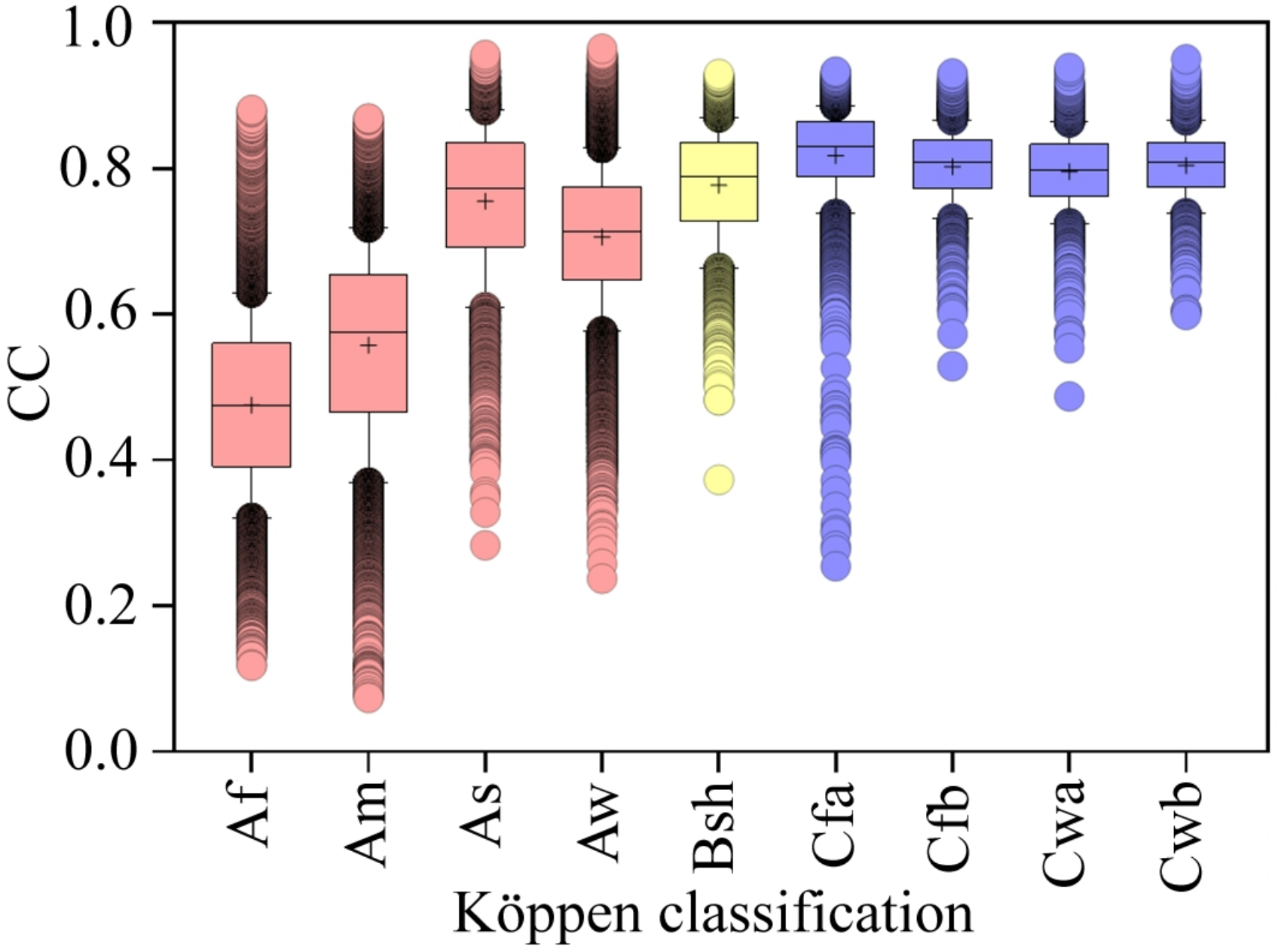
1.0
0.8
0.6
0.4
0.2
0.0
CC
Af
Am
As
Aw
Bsh
Cfa
Cfb
Cwa
Cwb
Köppen classification

Table 1 Summary of relevant studies that evaluated the IMERG products at country-wide scale in relation to the proposed study.

Study	IMERG Products	Location / study area	Study period	Number of gauges	Analysis approach
1. Tan and Duan (2017)	Final Run	Singapore / 719.9 k km^2	1/Apr/2014 to 31/Jan/2016	48	Point-cell
2. Muhammad et al. (2018)	Late Run and Final Run	Pakistan / 796.1 k km^2	1/Jan/2015 to 31/12/2016	36	Point-cell
3. Mahmoud et al. (2018)	Early Run, Late Run, and Final Run	Saudi Arabia / 2.1 M km^2	1/Oct/2015 to 30/Apr/2016	189	Point-cell
4. Tang et al. (2016)	Early Run, Late Run, and Final Run	China / 9.3 M km^2	1/Apr/2014 to 31/Dec/2014	2200	Grid box
5. Prakash et al. (2018)	Final Run	India / 3.3 M km^2	1/Jun/2014 to 31/Sep/2014	7000	Grid box
6. Tan and Santo (2018)	Early Run, Late Run, and Final Run	Malaysia / 338 k km^2	12/Mar/2014 to 29/Feb/2016	501	Point-cell
7. Rozante et al. (2018)	Final Run	Brazil / 8.5 M km^2	1/Apr/2014 to 28/Feb/2017	3400	Point-cell
8. Asong et al. (2017)	Final Run	Southern Canada / 6.1 M km2	12/Mar/2014 to 31/Jan/2016	732 and CaPA gridded product	Point-cell and grid box
9. This study	Final Run	Brazil / 8.5 M km^2	1/Jan/2016 to 31/Dec/2016	4911	Grid box

Table 2 Definition of rainy and non-rainy days for IMERG-V05 and observed data.

		Gauge	
		Rain	No rain
IMERG-V05	Rain	A	B
	No rain	C	-

Supplementary material for

Grid box-level evaluation of IMERG over Brazil at various space and time scales

André N. Gadelha[a,*], Victor Hugo R. Coelho[a,*], Alexandre C. Xavier[b], Luís Romero Barbosa[a,c], Davi C. D. Melo[d,e], Yunqing Xuan[f], George Huffman[g], Walt Petersen[h], Cristiano das N. Almeida[a]

[a] Department of Civil and Environmental Engineering, Federal University of Paraíba, João Pessoa, PB 58051-900, Brazil

[b] Department of Rural Engineering, Federal University of Espírito Santo, Alegre, ES 29075-910, Brazil

[c] Institute of Earth and Environmental Science, University of Potsdam, Potsdam, BB 14476, Germany

[d] Department of Soils and Rural Engineering, Federal University of Paraíba, Areia, PB 58397-000, Brazil

[e] Department Hydraulics and Sanitary Engineering, University of São Paulo, São Carlos, SP 13566-590, Brazil

[f] College of Engineering, Swansea University, Bay Campus, Swansea SA1 8EN, UK

[g] NASA Goddard Space Flight Center, Greenbelt, MD 20771, USA

[h] NASA Marshall Space Flight Center, Huntsville, AL 35805, USA

Equations S1 (Relative ME) and S2 (Relative RMSE)

The relative (R) errors for both ME and RMSE metrics are:

$$\mathrm{RME} = \frac{\frac{1}{\mathrm{N}}\sum_{\mathrm{n}=1}^{1}(\mathrm{E_i} - \mathrm{O_i})}{\frac{1}{\mathrm{N}}\sum_{\mathrm{n}=1}^{1}\mathrm{O_i}} \times 100 \qquad \text{Eq. (S1)}$$

$$\mathrm{RRMSE} = \frac{\sqrt{\frac{1}{\mathrm{N}}\sum_{\mathrm{i}=1}^{\mathrm{n}}(\mathrm{E_i} - \mathrm{O_1})^2}}{\frac{1}{\mathrm{N}}\sum_{\mathrm{n}=1}^{1}\mathrm{O_i}} \times 100 \qquad \text{Eq. (S2)}$$

where O is the observed rainfall (mm), E is the IMERG-V05 estimated rainfall (mm), i is the index of the number of pairs, and n is the total number of compared pairs. Both relative ME and relative RMSE measure the precision of the IMERG-V05 product in relation to observed rainfall, so values close to zero percent

indicate smaller deviations. However, the relative ME gives an overall indicator of the bias (positive or negative), with the disadvantage that the positive and negative errors can cancel each other. Hence, sometimes a small ME does not means minor errors. On the other hand, the relative RMSE gives an idea of estimate errors that is influenced by the sample size, tending to small results when increasing the n.

Figures S1 to S3

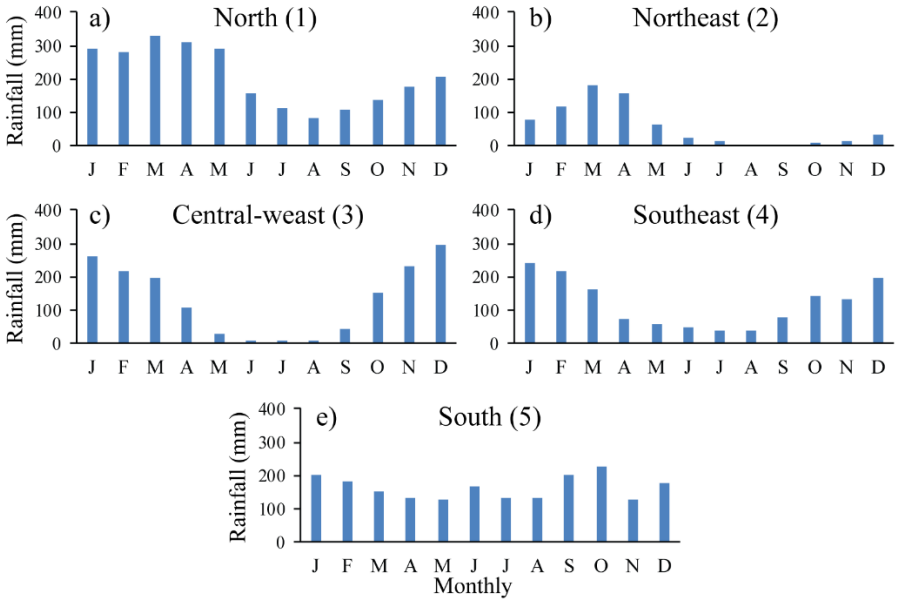

Fig. S1 Long-term monthly average rainfall obtained from rain gauges within the five selected subareas: (a) North, (b) Northeast, (c) Central-west, (d) Southeast, and (e) South.

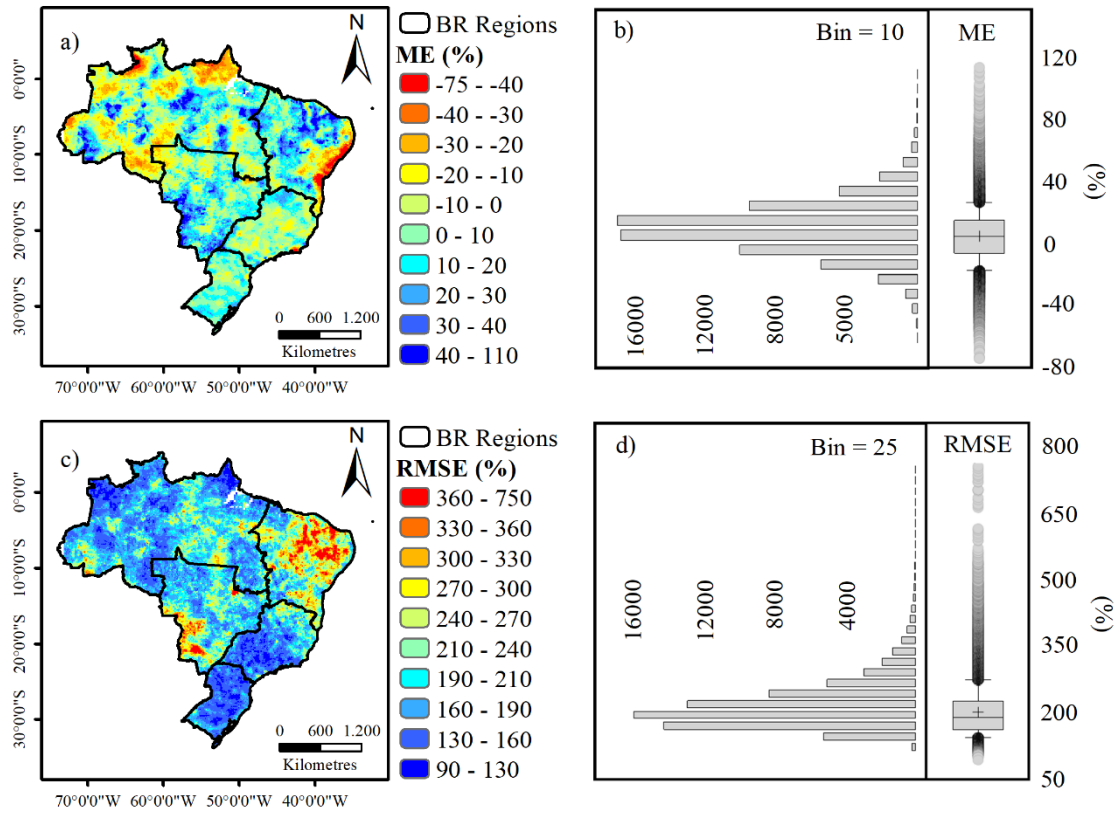

Fig. S2 Spatial distributions of daily relative (a) ME and (c) RMSE**.** Box plots and histograms of daily relative (b) ME and (d) RMSE.

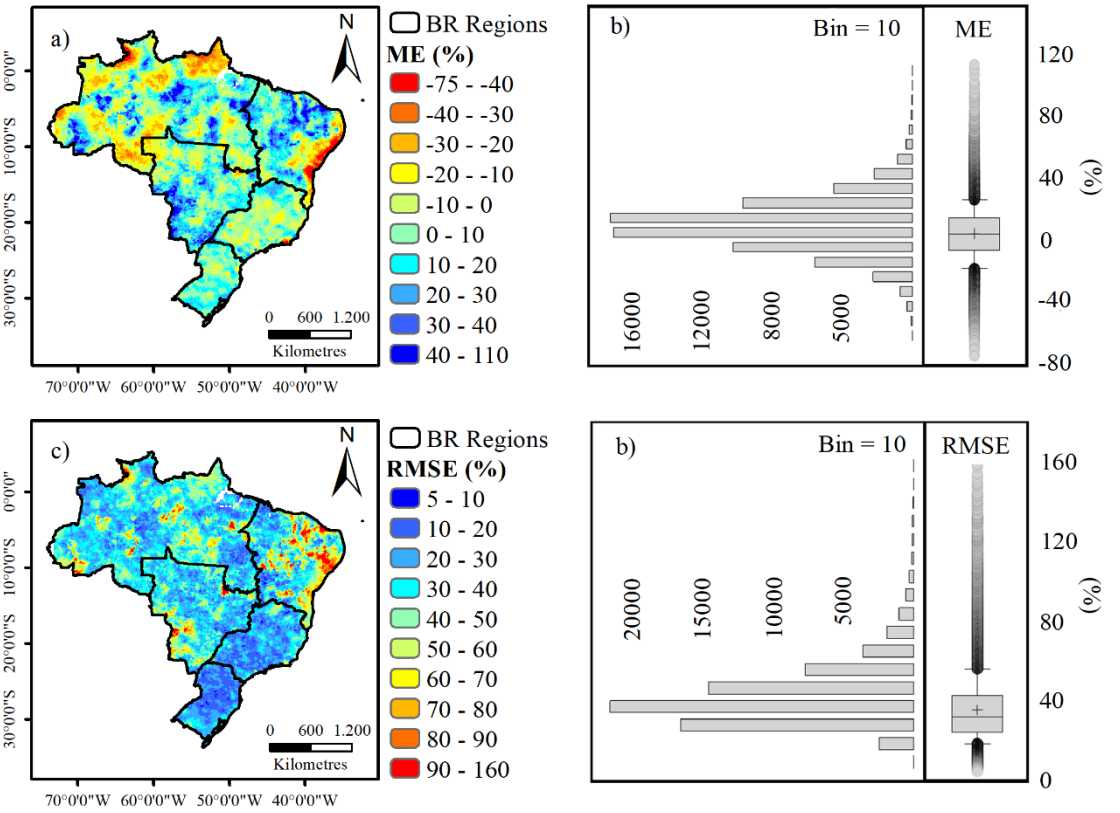

Fig. S3 Spatial distributions of monthly relative (a) ME and (c) RMSE**.** Box plots and histograms of monthly relative (b) ME and (d) RMSE.

Table S1

Table S1 Relative values of ME and RMSE for the subarea analysis at daily and monthly time scales.

Region	Daily		Monthly	
	Relative ME	**Relative RMSE**	**Relative ME**	**Relative RMSE**
North (1)	7.4%	93.9%	7.4%	11.6%
Northeast (2)	32.3%	196%	32.2%	47.4%
Central-west (3)	6.0%	88.1%	6.0%	13.6%
Southeast (4)	1.3%	96.5%	1.3%	8.7%
South (5)	0.7%	97.1%	0.6%	14.7%